MULTISCALE ANALYSIS OF A MIGRATING SUBMARINE CHANNEL SYSTEM IN A TECTONICALLY-CONFINED BASIN: THE MIOCENE GORGOGLIONE FLYSCH FORMATION, SOUTHERN ITALY

Casciano C.I.[1], Di Celma C.[1], Patacci M. [2], Longhitano, S.G.[3], Tropeano M.[4], McCaffrey, W.D.[2]

[1] *Scuola di Scienze e Tecnologie, Sezione di Geologia, Università degli Studi di Camerino, Camerino, Italy*
[2] *Turbidites Research Group, School of Earth and Environment, University of Leeds, Leeds LS2 9JT, UK*
[3] *Dipartimento di Scienze, Università della Basilicata, Potenza 85100, Italy*
[4] *Dipartimento di Scienze della Terra e Geoambientali, Università degli Studi di Bari "Aldo Moro", Bari, Italy*

ABSTRACT

The Miocene Gorgoglione Flysch Fm records the stratigraphic product of protracted sediment transfer and deposition through a long-lived submarine channel system developed in a narrow and elongate thrust-top basin of the Southern Apennines (Italy). Channel-fill deposits are exposed in an outcrop belt approximately 500 m thick and 15 km long, oriented nearly parallel to the axis of the former basin. These exceptional exposures of channel strata allow the stacking architectures and the general evolution of the channel system to be analysed at multiple scales, deciphering the effects of syn-sedimentary thrust tectonics and basin confinement on the depositional system development. Two end-member types of elementary channel architectures, each consisting of a distinct internal facies distribution, stratal patterns and associated out-of-channel heterolithic deposits, have been identified: (i) high aspect-ratio, weakly-confined channels; and (ii) low aspect-ratio, strongly-confined channels. Their systematic stacking results in a complex pattern of seismic-scale depositional architectures that composes the stratigraphic framework of the turbidite system and controls its reservoir-scale heterogeneity. From the base of the succession, two prominent channel-complex sets have been recognised, overlain by isolated channels and channel complexes incisional into mud-prone slope deposits. This marked juxtaposition of different channel architectures is interpreted to have been governed by the regional thrust tectonics, in combination with a high subsidence rate that promoted significant aggradation. In this scenario, the alternate in- and out-of-sequence tectonic pulses of the basin-bounding thrust structures controlled the activation of the coarse-clastic inputs in the basin and the resulting stacking architectures of the channelised units. The tectonically-driven confinement of the depositional system limited the lateral offset in channel stacking, preventing large-scale avulsions. This study should find wide applicability in analogous depositional systems in the subsurface, facilitating the characterization of hydrocarbon reservoirs whose hosting architecture has been influenced by tectonically-controlled lateral confinement and associated lateral tilting.

1. INTRODUCTION

Coarse-grained sediments are generally transported into the deep-marine realm through an interconnected network of variously sized submarine channels (Mutti and Normark, 1987; Clark and Pickering, 1996; Peakall and Sumner, 2015). Commonly, channel architecture records a protracted history of incision and deposition at multiple scales related to different types of sediment-gravity flows (Hubbard et al., 2014). The main features of the sediment-gravity flows, such as magnitude and both density and type of transported sediment, may vary as a consequence of changes in allogenic (e.g., tectonics, sea-level fluctuations) and autogenic (e.g., channel avulsions) factors (Kneller, 2003; Pirmez et al., 2000; Sylvester and Covault, 2016; Jobe et al., 2016).

Despite the crucial role of submarine channels for the dynamics of sediment-routing systems and their importance as hydrocarbon reservoirs, the complex interactions between the mechanisms of sediment transport and the character of the associated submarine channel systems remain still poorly understood (Samuel et al., 2003; Porter et al., 2006; McHargue et al., 2011). The detailed characterization of turbidite channels, in terms of depositional geometries, grain-size distributions, connectivity, net-to-gross trends and facies associations, has important implications for the development of efficient exploration and production strategies in the petroleum industry (Brunt and McCaffrey, 2007; Covault et al., 2016). Recent advances in seismic stratigraphy applied to conventional and high-resolution three-dimensional datasets offered a compelling method for understanding the large-scale geometries and stacking patterns of submarine channels (e.g., Mayall and Stewart, 2000; Posamentier and Kolla, 2003; Deptuck et al., 2003; Babonneau et al., 2010; Janocko et al., 2013). However, the spatial variability of reservoir properties is associated with small-scale differences in the nature of channel fills, occurring at scales below the resolution of 3D seismic datasets. For this reason, over the past years, numerous studies have focused on the details of suitable outcrop analogues to improve the sub-seismic characterization of intrachannel stratal complexities (e.g. Navarro et al., 2007; Kane et al., 2009; Pyles et al., 2010; Di Celma et al., 2011; Thomas and Bodin, 2013; Li et al, 2016). In spite of their general 2D nature, the detailed characterization of outcrop analogues represents a powerful tool to resolve the internal anatomy of turbidite channels, improving our knowledge on the sedimentary facies distribution and on the associated depositional processes (e.g., Beaubouef, 2004; Schwarz and Arnott, 2007; Figueiredo et al., 2013).

However, relating the observations made at the outcrop scale on ancient turbidite successions to the architectural styles of modern and subsurface deposits vividly imaged in 3D seismic datasets can be challenging (e.g., Mutti and Normark, 1987; McHargue et al., 2011). This is largely due to differences in resolution between outcrop and seismic data, and limited well control to bridge the resolution gap (Deptuck et al., 2003). Moreover, outcrop analogues are rarely extensive enough to allow for a broad-scale perspective of the depositional system (Beaubouef, 2004; Van der Merwe et al., 2014). The Upper Miocene Gorgoglione Flysch (GF) Formation represents an exception to this common situation. This extraordinarily-preserved turbidite succession, deposited within a thrust-top basin of the Southern Apennines of Italy (Fig. 1), offers an excellent opportunity to investigate submarine channel architectures developed in tectonically active deep-water settings, from their small-scale facies architecture to their large-scale stacking pattern.

A primary objective of this study is to verify the predictability of the architectural geometries observed at the seismic scale (i.e., hundreds to thousands of meters) from the depositional features documented at the sub-seismic scale (i.e., centimeters to tens of meters). For this purpose, the stratal hierarchy of the turbidite system is explored through the detailed characterization of channel-fills and flanking out-of-channel deposits, and the interpretation of their spatial distribution across the outcrop belt. The effects of the basin configuration and syn-sedimentary thrust tectonics on the evolution of the depositional architectures are assessed. Finally, a model for deep-water sedimentation in elongate thrust-top basins is proposed, where the observed stratigraphic occurrence of different architectural styles is interpreted to reflect a progressive shift of the turbidite system along the depositional profile. This model should find wide applicability in other basins, particularly those formed at tectonically active margins, and may have direct implication for the exploration of hydrocarbon resources in regions where deep-water channel reservoirs developed in confined settings.

2. STUDY AREA AND GEOLOGICAL SETTING

The Southern Apennines are a prominent thrust-and-fold belt developed from late Oligocene to Pleistocene on a W-dipping subduction zone, in the general framework of African and Eurasian major plates convergence (Gueguen et al., 1998; Patacca and Scandone, 2007). The resulting north-eastward migration of the orogenic thrust front determined the progressive involvement in the thrust belt of several intervening Meso-Cenozoic basin and platform successions covering the Adria passive margin and adjacent Tethyan ocean (Patacca and Scandone, 2007 and references therein). Accordingly, the structure of the Southern Apennine accretionary wedge is configured as a thick thrust pile of heavily deformed rootless nappes, tectonically overlying a buried deep-seated carbonate duplex system (Vezzani et al., 2010 and references therein).

Syn-tectonic thrust-top basins of upper Eocene to Plio-Pleistocene age, progressively were filled by coarse clastic sediments derived from the emerged areas of the chain, unconformably covering the whole thrust-pile and preserving the older structures of the thrust system (Patacca and Scandone, 2007; Vezzani et al., 2010). One of the better-preserved thrust-top depositional units of the Southern Apennines is the Gorgoglione Flysch (GF) Formation, an approximately 2 km thick turbidite succession that crops out in the eastern sector of the thrust belt. Main exposures of the GF succession occur in two broad areas, 150 km SE of Naples, in southern Italy (Fig. 1). Along the eastern edge of the former turbidite basin, the GF succession unconformably overlies the Cretaceous-Eocene mud-rich units of the Argille Varicolori Formation, which represents the deformed substrate (Fig. 1; Boiano, 1997). The deep-water strata of the GF succession mainly consist of coarse-grained sandy turbidites and mudstones with subordinate conglomerates, forming a prominent channel system developed within a narrow and elongate, NNW-SSE-trending basin (Boiano, 1997), oriented nearly parallel to the mean trend of Apennine thrust faults (Fig. 1). The overall physiography and the sedimentary evolution of the basin were controlled by contractional tectonics affecting the Southern Apennine accretionary wedge during the late Miocene (Pescatore, 1978;1988). The turbidite succession was deposited from the late Burdigalian to the Tortonian (Giannandrea et al., 2016), with variable degrees of lateral confinement, mainly provided by the developing orogen to the W and by the incipient outer thrust structures of the thrust-and-fold belt to the E (Pescatore et al., 1999; Butler and Tavarnelli, 2006). Provenance data show that the GF was sourced from a crystalline basement terrane located within the growing orogen to the west (Critelli and Loiacono, 1988; Critelli et al., 2017). However, paleocurrent indicators document a prevalent paleoflow direction from NNW to SSE, along the longitudinal axis of the basin (Loiacono, 1974). Accordingly, many authors invoked a paleogeographic scenario with sediment-gravity flows originated from an inferred shelf in the orogenic hinterland, which were directed down a NE-facing paleoslope and successively deviated toward SSE along the basin axis near the base of slope (Loiacono, 1993; Boiano, 1997).

In this study, the seismic-scale architecture and the outcrop-scale depositional features of the GF succession have been investigated across a NNW-SSE-oriented outcrop belt, approximately 500 m high and 15 km long, exposed near the towns of Pietrapertosa and Castelmezzano (Fig. 2A). The study area, located in the northern sector of the GF basin, is characterized by a well-exposed monoclinal structure, dipping to SW of approximately 40° and striking along a NW-SE direction, which defines an elongate ridge, oblique to the main sediment dispersal direction (Fig. 2B). The monocline represents the eastern flank of the NNW - SSE trending syncline (Fig. 1) in which the GF formation has been deformed during the post-Tortonian contractional tectonic phase of the Southern Apennine orogenic wedge (Piedilato and Prosser, 2005; Cavalcante et al., 2015).

3. METHODOLOGY

The deep-water strata of the GF system have been studied using both standard sedimentary facies analysis and emerging digital field techniques for outcrop mapping and data collection (Pitts et al., 2017). Traditional methods included bed-scale characterization of sedimentological and stratigraphic elements and paleoflow analysis. Twenty main stratigraphic sections were measured at cm to dm-scale (Fig. 2A) to document key sedimentary features such as grain size and sorting, primary sedimentary structures, bedding thickness and the nature of bed contacts, which form the basis for facies analysis. The position of the measured sections was chosen based on the best-exposed and most readily accessible locations. The lateral spacing between the sections is variable, ranging between 100 and 750 m, with additional shorter sections measured where necessary in order to characterize lateral changes in stratigraphic architecture over short distances (i.e., tens of meters). Logging was performed using a meter-scale folding-tape measure and a 2.1 m high Jacob's staff, instrumented with an integrated laser pointer, which allowed an improved accuracy in thickness measurements (Patacci, 2016). Paleoflow data were recorded across the entire outcrop belt from 973 paleoflow indicators, such as sole marks, ripple-marks, and cross-stratification. The log data were compiled into a database. For each bed, these data included thickness, stratigraphic height of base and top, lithology (i.e., sandstone vs. mudstone), facies type, average basal grain size and paleocurrent type and direction. This dataset allowed an array of secondary parameters to be determined, such as sandstone to mudstone ratio, average grain size and bed thickness. Pie charts of facies abundance were employed to contrast different stratigraphic intervals of the studied sections and to compare their facies distribution.

Additional digital data collection methods included the construction of ultra-high resolution outcrop panoramas produced by the GigaPan® imagery system and 3D outcrop models produced from aerial and ground based imagery using 3D photogrammetry, built to aid in the identification of key surfaces and depositional architectures (Pitts et al., 2017). GigaPan® images permit visual examination of geologic features on a computer screen with a high level of detail, comparable to that observable in the field. Three-dimensional photogrammetric models, created with Agisoft Photoscan® software for key stratigraphic sections, have been crucial to assess the spatial architectural variability of the depositional elements in detail.

4. LITHOFACIES RESULTS

The GF deep-water succession consists of a wide range of sedimentary facies, which have been distinguished on the basis of macroscopic sedimentological criteria (Bouma, 1962; Allen,1963; Lowe, 1982; Larue and Provine, 1988; Mutti, 1992; Kneller and McCaffrey, 2003; Talling et al., 2012) and are described and interpreted in Table 1. The sedimentary facies include: (i) Matrix-supported extra- and intra-formational conglomerates (LF 1; Fig. 3A, B); (ii) Structureless, commonly amalgamated, coarse-grained sandstones (LF 2; Fig. 3C, D); (iii) Structured, coarse-grained deposits, including planar-laminated sandstones (LF 3; Fig. 3E) and cross-stratified sandstones (LF 4; Fig. 3F); (iv) A wide spectrum of thin-bedded, “classical” Bouma-type turbidites (form LF 5 to LF 10; Fig. 3G, H, I, L, M, N); (v) Deformed and contorted sandstone beds (LF 11); and (vi) Mudstones and fine-grained siltstones (LF 12).

The composition of sandstones and conglomerates is quartzo-feldspathic, indicating a source dominated by granitic and gneissic metasedimentary rocks, carbonatic and siliceous sedimentary rocks, and minor felsitic and silicic volcanics (Critelli and Loiacono, 1988; Critelli et al., 2017). The textural and compositional immaturity of the GF sandstones has been associated with a rapid erosion of the source-rock and a general high sedimentation rate in the basin (Critelli and Loiacono, 1988).

The sedimentary facies are considered to be the basic ‘building blocks’ of the sedimentary succession (Walker, 1984) and represent the basis for an interpretation of the various modes of sediment deposition. Based on their spatial arrangement and depositional architecture, three main facies associations have been recognized. Their spatial distribution across the study area has been represented in a geological map illustrating the main depositional architectures (Fig. 4).

4.1. Facies association 1 (F.A.1) - Sandy and gravelly amalgamated deposits

Description. F.A.1 is characterized by a systematic distribution of vertically-stacked coarse-grained facies arranged in a crude fining-upward trend, commonly overlying prominent concave-upward erosional surfaces (Fig. 5). These facies include: a basal, matrix-supported conglomerate (LF 1), grading upward into thick, structureless amalgamated sandstones (LF 2) and planar-laminated sandstones (LF 3), abruptly capped by multiple orders of large-scale cross-stratified sandstones (LF 4) or by thick packages of structured, fine-grained sandstones (LF 6 and LF 8) and subordinate massive sandstones (LF 5). The proportions of these facies are highly variable between the studied sections where F.A.1 has been documented, with some components locally reduced or even missing. Single F.A.1 sediment packages are typically characterized by slightly undulated tops and sharp concave-upward bases producing rough lenticular geometries. Primary basal surfaces exhibit steep notches, which configure a “step-and-flat” cross-sectional geometry (Fig. 5A, B), and are locally ornamented by sole structures up to 20 cm long and minor loading features (Pitts et al., 2017). Subordinate erosional surfaces mantled by LF 1 conglomerates are widely documented within the primary basal surfaces, truncating the underlying coarse-grained beds of F.A.1.

Interpretation. Based on the three-dimensional arrangement of the coarse-grained facies, F.A.1 sandbodies have been attributed to processes of erosion, sediment bypass and ultimately filling of submarine channels (e.g., Mutti and Normark, 1987; Gardner and Borer, 2000). Concave upward basal surfaces are sculpted by multiple incisional gravity flows that passed through the channel and transported much of their sediment load basinward, leaving behind chaotic conglomerate-rich lag deposits (LF 1) that drape the channel base (Barton et al., 2010). Matrix-supported conglomerates dominate the channel axis and off-axis and denote the substantial erosion and sediment bypass that affect these portions of the channelforms (Hubbard et al., 2014; Stevenson et al., 2015). Abundant extra-formational conglomerates (LF 1A) are commonly confined within the deepest portions of the erosional channelforms (Fig. 5A) and are interpreted to characterize the channel axis setting (e.g., Camacho et al., 2002; Di Celma et al., 2011) and to indicate the channel thalweg (Thomas and Bodin, 2013). Conversely, their absence associated with a corresponding increase of intra-formational mudclast conglomerates (LF 1B; Fig. 5B), suggests deposition within a channel off-axis setting (Hubbard et al., 2014). Intra-formational mudstone clast breccias are commonly attributed to “rip-up” processes, as mudclasts are incorporated into the bypassing flows after turbulent scouring of the substrate (Butler and Tavarnelli, 2006).

Numerous secondary erosional surfaces draped by conglomeratic lags are observed within the primary confinement and are particularly well developed in the channel axis. These subordinate surfaces are suggestive of short-lived periods of flow bypass or erosion punctuating the main channel-fill phase (Beaubouef et al., 1999; Stevenson et al., 2015; Li et al., 2016).

Channel-axis stratigraphy is dominated by amalgamated, thick-bedded structureless sandstones with sparse granule- to pebble-sized clasts (LF 2B; Fig. 5A), resulting from rapid deposition by collapsing sand-rich high-density turbidity currents (e.g., McCaffrey and Kneller, 2004; Hubbard et al., 2014). Upward in channel-fill stratigraphy and laterally towards the channel margins, a gradual transition to less amalgamated, clean massive sandstones (LF 2A) and plane-parallel laminated sandstones (LF 3) occurs. In the channel margin setting, the limited occurrence of internal erosional surfaces, together with poorly developed sole structures, indicates that sediment-gravity flows were only partially erosive. However, the presence of LF 2A sandstones associated with high fall-out rates from high-density turbidity currents (Lowe, 1982), suggests that these flows were rapidly declining from erosional to depositional (Li et al., 2016).

Large-scale, cross-stratified deposits (LF 4) capping the channel-fill successions (Fig. 5C) have been interpreted to record the final phases of channel infill, with the progressive reduction of channel confinement leading to the formation of relatively fast and dilute, fully turbulent flows. Multiple orders of superimposed cross-sets record a variable range of paleocurrent directions, diverging up to 75° from the mean paleoflow determined by the sole structures beneath channel-fill packages. These divergent paleoflow trends are consistent with a partial lateral flow expansion as channel confinement progressively decreases. Alternatively, the different large-scale cross sets at the channel top can be related to the final channel filling by three-dimensional bedforms such as sandwaves, as invoked by Brunt and McCaffrey (2007) for the turbidite channels of the Grès du Champsaur (southern France). Within the GF channels, the progressive compensation of the channel top irregularities by multiple stacked three-dimensional bedforms might have resulted in distinct superimposed orders of cross-sets with different paleoflow directions.

Where the capping cross-stratified interval is absent, the top of channel-fill successions comprises abundant planar-laminated and ripple cross-laminated, fine-grained sandstones (LF 6 and LF 8, respectively) and subordinate massive sandstones (LF 5) alternating with mudstones (Fig. 5D). These sediments and the upward decrease in the degree of amalgamation suggest a progressive decline in sand concentration, volume and energy of the flows in the channel conduit (Hubbard et al., 2014).

4.1.1 Fundamental types of channel architecture

The distribution of the channel-fill facies, together with the nature of their flanking out-of-channel deposits, show a substantial variability across the study area. These variable depositional features have been interpreted to be associated with two end-member types of elementary channel architectures: weakly-confined channels and strongly-confined channels. Similar architectural styles have been documented in other ancient turbidite systems, such as the Permian Laingsburg Formation of the Karoo Basin (Brunt et al., 2013b) or the upper Cretaceous Tres Pasos Formation of the Magallanes Basin (Pemberton et al., 2016).

Weakly-confined channels. These channelized sedimentary bodies are typically 5 – 17 m thick, occasionally up to 20 m. Amalgamated LF 2B sandstones are prevalent within the channel axes, but less amalgamated LF 2A and LF 3 sandstones become dominant towards the channel margins, directly overlaying the primary channelform surfaces. Basal channel surfaces are mantled exclusively by thick packages of matrix-supported mudclast conglomerates (LF 1B), with rare extra-formational conglomerates (LF 1A), and show a significant decrease in erosional character towards the marginal areas of the channel-form.

The axis to margin facies transition and the poorly-erosional nature of the basal surfaces at the margins suggest relatively high energies in channel thalwegs and progressively lower energies towards marginal areas (Navarro et al., 2007; Pemberton et al., 2016). Flows traversing weakly-confined channels are interpreted to have been larger than the axial confinement. These flows over-spilled their initial lateral confinement and formed proximal sand-rich overbank deposits (F.A.2; see below) that progressively aggraded (e.g., Arnott et al., 2011; Brunt et al., 2013b). Overbank aggradation slightly increased the confinement of the large turbidity flows, with a progressive reduction of the volume of overspill that resulted in thinning-upward trends (e.g., Kane et al., 2007; Kane and Hodgson, 2011), locally documented within F.A.2 heterolithic packages (Fig. 6A; see below).

Strongly-confined channels. Typically, strongly-confined channels are 13-26 m thick and 180-450 m wide, with aspect ratios between 10 and 30 (Pitts et al., 2017). These dimensions are consistent with low-aspect-ratio slope channels reported in literature for other deep-water systems (McHargue et al., 2011). Strongly-confined channel fills display a marked multistorey architecture and are relatively coarser-grained than weakly-confined channels. LF 2B sandstones dominate the majority of channel element's infill, with subordinate LF 2A sandstones only relegated towards the marginal areas. Strongly-confined channel are commonly flanked by, and deeply incisional into, thick packages of mud-prone heterolithic deposits of F.A.3 (see below).

The spatial distribution of the channel-fill facies and the fine-grained nature of the out-of-channel deposits are indicative of high-energy incisional flows sculpting deep erosional conduits and becoming strongly confined by the resulting morphologies (e.g., Brunt and McCaffrey, 2007; Hubbard et al., 2014; Pemberton et al., 2016).

4.2. Facies association 2 (F.A.2) - Sand-prone, heterolithic deposits

Description. F.A.2 packages (Fig. 6A) typically flank the weakly-confined channel-fill deposits, showing a progressive upward and lateral transition into mud-prone thin-bedded heterolithic deposits of facies association 3 (F.A.3). They consist of alternating thin- to medium-bedded sandstones (facies LF 5 to LF 10) and mudstones (LF 12), with occasional folded and contorted deposits (LF 11), organized in well-stratified packages (Fig. 6A). The resulting net-to-gross ratio is commonly greater than 40% (Fig. 4B). Massive Ta-dominated beds (LF 5), represent about 40% of the total F.A.2 volume, with subordinate Tb - and Tc-dominated beds (LF 6 and LF 8, respectively; Fig. 4B). Sandstone beds range from 10 to 70 cm thick and are typically tabular, showing a rather constant bed thickness at the outcrop scale (ca. 100 m). Bed bases are commonly flat or weakly erosive into the underlying mudstones. Bed amalgamation is rare.

Sandstone beds are abruptly overlain by thin (1-5 cm) layers of mudstone or fine siltstone (LF 12). Mudstone beds show an average thickness of 3.3 cm and their relative volumetric abundance in F.A.2 packages is around 16% (Fig. 4B).

Interpretation. The stratigraphic distribution of F.A.2 deposits adjacent and among the amalgamated paleo-channelized bodies (Fig. 4) indicates overbank deposition by widespread, moderate- to low-concentration turbidity currents overflowing an active channel (Hansen et al., 2015). F.A.2 overbank deposits are relatively sand-rich. The relative abundance of massive LF 5 sandstones, together with little evidence of erosion and bed amalgamation within F.A.2 packages, are diagnostic of an overbank position proximal to the associated channel (Kane et al., 2007; Migeon et al., 2012).

4.3. Facies association 3 (F.A.3) - Mud-prone heterolithic deposits

Description. Thin-bedded packages of alternating fine- to very-fine grained sandstone beds and mudstone or siltstone beds characterize F.A.3 (Figs. 4C, 6B). The resulting net-to-gross ratio ranges from 10 to 20%, with local maximum values of 35%, considerably lower than in F.A.2 packages. Mudstone or siltstone intervals (LF 12) are dominant, representing about the 60% of the total F.A.3 (Fig. 4C) with an average thickness of c. 10 cm, occasionally up to 30 cm. Sandstone beds are typically up to 6 cm thick, showing a tabular geometry at the outcrop scale (10s of meters). They mainly consist of abundant ripple cross-laminations or mm-thick parallel laminations (LF 8 and LF 6, respectively). Massive sandy beds of facies LF 5, up to 50 cm thick and weakly erosional into the muddier substrate, locally occur within the mud-prone packages, displaying lenticular geometries at the scale of the tens of meters (Fig. 6B).

Interpretation. The sedimentological features of the mud-prone heterolithic deposits suggest their formation under relatively low-energy conditions, with two plausible origins: (i) background slope deposits (e.g., Figueiredo et al., 2010), occasionally incised by slope channels or ii) channel-overbank strata (e.g. Kane and Hodgson, 2011). In the first interpretation, the thin tabular sandstone beds were deposited by volumetrically small and dilute low-density turbidity currents. Lenticular beds of facies LF 5 can be interpreted as shallow scour-fill deposits, indicating fluctuations in the volumes of turbidity currents in the slope environment. In the second scenario, the deposition of thick, mud-dominated packages can be interpreted to result from far-travelling and dilute over-spilling turbidity currents reaching distal overbank areas, which deposited most of their coarser-grained sediment load in more proximal overbank areas (Kane et al., 2007). Alternatively, mud-prone overbank deposits may also result from the overspill of the upper, more dilute portion of highly-confined flows traversing the channels (Hiscott et al., 1997). In this case, the lower sand-rich parts of the gravity flows are not able to escape their strong lateral confinement, resulting in the virtual absence of sediment coarser than fine-grained sand in the overbank strata (Arnott et al., 2011).

5. ARCHITECTURAL AND SEDIMENTOLOGICAL VARIABILITY

5.1 Channel hierarchy

In the study area, due to their heterolithic and relatively fine-grained nature, F.A.2 and F.A.3 deposits commonly weather recessively and are often covered by vegetation. Conversely, channel-fill deposits of F.A.1 crop out extensively, forming spectacular cliffs (Fig. 2B) that allowed the detailed architectural characterization of the channelized units. For this purpose, a hierarchical approach is essential, facilitating the recognition and interpretation of persistent patterns at multiple scales (e.g., Ghosh and Lowe, 1993; Di Celma et al., 2011; Macauley and Hubbard, 2013; Stright et al., 2014). The stratigraphic hierarchy used in this study is based on the schemes proposed by Campion et al. (2005) and Sprague et al. (2005).

The two basic types of channel-fill depositional architectures documented in the study area represent channel elements, considered as the fundamental building blocks of submarine channel systems (Beaubouef, 2004). Individual elementary channels define distinct conduits for relatively confined flows (Mutti and Normark, 1987; Clark and Pickering, 1996) and are commonly dissected by secondary erosion surfaces bounding discrete fill phases, called “stories”, that are up to 2 m thick. The vertical or horizontal stacking of multiple, genetically-related channel elements with similar architectural style and lithofacies organization constitute a single channel-complex. These architectural units in the GF succession are up to 85 m thick, comparable to other channel complexes documented in literature (e.g. Stright et al., 2014; Bain and Hubbard, 2016). Where multiple genetically-related channel complexes are stacked in a consistent pattern, they form a single channel complex-set. In this study, the recognized channel complex-sets are approximately 100 to 300 m in thickness. Comparable dimensions have been reported by Beaubouef (2004) in the Late Cretaceous Cerro Toro Formation (Magallanes Basin, Chile) and Thomas and Bodin (2013) in the Finale channel system of the Numidian Flysch Formation (Sicilide Basin, southern Italy).

5.2. Seismic-scale architectural units

Weakly-confined and strongly-confined elementary channels effectively control the depositional architectures developed by the large-scale channelized units of the GF system (Fig. 7). In the study area, two prominent channel complex-sets have been recognized: CS 1 and CS 2 (Fig. 7), composed of multiple stacked and amalgamated channel complexes, laterally associated with thick sand-prone (F.A.2) and mud-prone (F.A.3) heterolithic deposits. Directly above the CS 2, isolated channels and channel complexes occur, representing the dominant architectural unit in the upper portion of the turbidite succession, where they are embedded within and, markedly incisional into, mud-prone heterolithic deposits of F.A.3.

These architectural units are described from the base to the top of the GF succession, including their location, large-scale lithological variability of channel-fills and associated out-of-channel deposits, and main internal stratigraphic surfaces, as well as other notable characteristics that inform paleo-environmental interpretations. Detailed characterization of the architectural units, together with the reconstruction of their stratigraphic relationships, is crucial to the interpretation of the evolutionary history of the GF turbidite succession.

5.2.1. Channel complex-set 1 (CS 1)

Description. CS 1 is an isolated channel complex-set that crops out at the base of the GF succession, in an area located at the confluence of the Caperrino Torrent with the Basento River (Figs. 4, 7). Field mapping reveals that, at the large scale, CS 1 outcrops have an irregular shape, elongated in NE-SW direction, with a maximum lateral extension of approximately 1200 m measured along strike (Fig. 4).

Channel-fill strata dip towards NW of approximately 70°, showing a comparatively higher dip-angle than those of the CS 2, which dip towards NW of about 40°. CS 1 unconformably overlies the clayey units of the Argille Varicolori Formation along an extensive irregularly-shaped stratigraphic contact (Fig. 4; Piedilato and Prosser, 2005).

CS 1 reaches a maximum thickness of nearly 100 m, resulting from the amalgamation and stacking of several, markedly incisional, strongly-confined channels. The distribution of the coarse-grained channel-fill facies (F.A.1) within this prominent channel complex-set reveals a crude fining-upward trend at the large scale. The lower ~ 75 meters are characterized by relatively abundant matrix-supported extrabasinal conglomerates (LF 1A) overlying concave-upward erosional surfaces, and subordinate coarse-grained sandstones (mostly LF 2B). This character gradually changes upward in the channel complex-set stratigraphy, with the upper ~ 25 meters recording a considerable reduction in the amount of LF 1A conglomerates and a concurrent increase of LF 2B and LF 3 sandstones coupled with a more evident stratification.

CS 1 is flanked by thinly-bedded, mud-prone heterolithic overbank deposits of F.A.3, with the outcrop extending laterally for about 7 km towards SE and about 3 km towards NW (Fig. 4). Moreover, a nearly 100 m thick package of F.A.3 mud-prone deposits occurs above the CS 1 (Fig. 7B), separating it from the base of the CC 2.

Interpretation. Previous studies interpreted the deposition of CS 1 coarse-grained sediments as the progressive infill of topographic irregularities on the basin floor (Loiacono, 1993; Boiano, 1997). However, the steep and irregular contact with the underlying clayey units of the substrate, along with the marked incisional character of the stacked strongly-confined channels, indicates an erosional origin for CS 1.

A potential source of coarse-grained sediments located to W-NW, in the hinterland of the orogenic wedge, has been invoked, possibly triggered by the early activity of the internal thrust structures that determined the uplift of the chain (Critelli and Loiacono, 1988; Loiacono, 1993). However, due to limited exposure, no direct paleoflow measurements from the base of the turbidite channels have been collected during this study to confirm this hypothesis.

The nearly 100 m-thick package of mud-prone heterolithic deposits (F.A.3) that separates CS 1 from the base of CS 2 is likely related to a progressive reduction of the coarse-grained clastic inputs feeding the CS 1, until their complete deactivation. This interpretation is consistent with the broad, crude fining-upward trend documented within the channel complex-set. The progressive shutdown of coarse-grained inputs is presumably associated with the early propagation of an incipient outer thrust of the Apennine thrust-and-fold belt, which must have tilted the CC 1 deposits before the deposition of the CS 2 to account for their different structural dip. According to Giannandrea et al. (2016), this tectonic structure developed at the Burdigalian-Langhian transition and marked the north-eastern boundary of the GF basin, which started to be configured as a narrow and NW-SE elongated thrust-top basin with a south-eastward dipping basin floor.

5.2.2. Channel complex-set 2 (CS 2)

Description. CS 2 crops out widely throughout the study area for up to 11.5 km, albeit with local discontinuous exposures (Fig. 2B). It consists of two broad channel belts, named CS 2A and CS 2B. The lower of the two channel belts (i.e., CS 2A) overlies an extensive erosional surface, markedly incisional into the underlying mud-prone deposits. At the large-scale, the outcrops of these channel belts show a pronounced elongated geometry in NNW-SSE direction along the axis of the basin, roughly parallel to the main paleoflow direction, and exhibit a convergence towards the N (Fig. 4), although the locus of the conjunction is not exposed. In the opposite direction, towards SSE they both display a progressive thinning, passing from a maximum thickness of 330 m north of the Castelmezzano village to nearly 35 m south of the Pietrapertosa village (Fig. 4).

CS 2A and CS 2B have similar sedimentological features and are characterized by a composite architecture, resulting from the amalgamation of several weakly-confined channel elements, laterally associated with sand-prone, heterolithic overbank deposits of F.A.2. Elementary channels stack with limited lateral offset (Fig. 8) to form channel complexes that typically range in thickness from 60 to 85 m and are separated by major erosional surfaces, laterally traceable for up to 4 km, as documented within the superbly exposed cliffs of CS 2B (Fig. 9). In its northern sector, four amalgamated, partially off-set stacked channel complexes have been recognized (Fig. 9). Here, channel-fills are dominated by poorly-sorted sandstones of facies LF 2B, with subordinate mudclast-rich conglomerates of facies LF 1B (Fig. 10). Channel complexes gradually thin towards SE, where increasingly thicker packages of tabular, sand-prone heterolithic deposits (F.A.2) occur and separate individual channelized units (Fig. 10). Further towards SE, amalgamated channel-fill deposits pass laterally into lenticular sandbodies, 6-19 m thick and laterally-persistent for up to 600 m (Figs. 4, 10). The reconstruction of their full lateral extension is difficult because of the occurrence of high-angle normal faults associated with post-depositional tectonic deformations affecting the GF succession (Fig. 4; Cavalcante et al., 2015) and that disrupt the original depositional geometries. These lenticular sandbodies are comprised of thick-bedded, clean massive sandstones (LF 2A) and planar-laminated sandstones (LF 3), directly overlying weakly-incisional basal surfaces. A similar lateral transition from amalgamated coarse-grained sandstones into extensive lenticular sandbodies has been also documented towards N, in the upper part of the CS 2B (Figs. 4, 10).

Interpretation. Due to their lateral extension, CS 2A and CS 2B represent important stratigraphic markers in the GF succession (Boiano, 1997). Previous workers interpreted them as two distinct systems, relating their formation to the combined effect of eustatic sea-level fall and basin modifications associated with the activity of the thrusts delimiting the turbidite basin to the NE (Loiacono, 1993; Boiano, 1997; Giannandrea et al., 2016). The thrust propagation produced a remarkable narrowing of the GF basin that influenced the large-scale depositional architectures of the developing sandbodies, as suggested by the NNW-SSE elongation of the channel belts, approximately in line with the mean paleocurrent direction reported by Loiacono (1993).

The convergence of the two channel belts observed in the norther sector of the study area (Fig. 4), together with their comparable sedimentological features, are indicative of architectural continuity and suggests that CS 2A and CS 2B represent a single channel complex-set, the CS 2, characterized by a systematic aggradation and lateral migration of its component units.

The depositional style of the CS 2 could have been established through a combination of allocyclically-driven seafloor degradation and aggradation through the protracted evolution of weakly-confined channels (e.g., Deptuck et al., 2003; Hodgson et al., 2011). Individual channel elements stack to form channel-complexes bounded by laterally-extensive basal erosion surfaces, likely resulting from an initial incisional phase, when high-energy, by-passing currents created an erosional conduit (e.g., Eschard et al. 2003; Beaubouef, 2004). After this initial phase, channel complexes became dominated by significant aggradation. This repeated process eventually resulted in the composite internal architecture of the CS 2, characterised by numerous stacked and amalgamated channel bodies (Fig. 8), whose occurrence is commonly identified as an evidence for prolonged sediment transfer (e.g. Di Celma et al., 2011; Sylvester et al., 2011).

In this scenario, the prominent erosional surface at the base of the CS 2A can be interpreted as the record of the master channel complex-set conduit (*sensu* Macauley and Hubbard, 2013; erosional valley surface *sensu* McHargue et al., 2011; submarine incised valley *sensu* Janocko et al., 2013) confining the CS 2. However, due to the high obliquity of the outcrop belt that provides only a longitudinal perspective of the master conduit geometry, the different processes active during the establishment of the master conduit (e.g. down-cutting, mass failure, external levee construction) cannot be ascertained from the available dataset.

The spatial distribution of the channel-fill facies across the CS 2B (Fig. 10) suggests that, in the northern sector of the channel belt, the axes and off-axes portions of the amalgamated, weakly-confined channels widely crop out. Towards the SE, these channels progressively transition into laterally-persistent, lenticular sandbodies (Fig. 4). Due to their position, downcurrent of the amalgamated channels, and to their apparent elongated geometry, previous workers interpreted these sandbodies as depositional lobes (e.g., Pescatore et al., 1980; Boiano, 1997). However, their relatively limited dimensions and internal sedimentological features are substantially different from the typical characteristics of submarine lobe deposits documented in the modern literature (e.g., Prélat et al., 2009; Etienne et al., 2012; Grundvag et al., 2014). In this study, the south-eastern lenticular sandbodies are interpreted to represent the margins of the stacked weakly-confined channels exposed in the northern part of CS 2B (Fig. 9). It seems likely that in the south-eastern portion of the study area, the channel axes are buried below the outcrop and therefore the channel margins become increasingly better exposed, intersecting the NW-SE oriented outcrop line (Fig. 10). The same interpretation of channel margin deposits can be invoked for the elongated lenticular sandbodies observed towards N, in the upper part of the CS 2B (Fig. 10).

5.2.3 Isolated channels and channel complexes

Description. In the study area, the upper portion of the GF formation is characterized by the widespread occurrence of isolated elementary channels and channel complexes (Fig. 7). Directly above the CS 2, these isolated channelform sedimentary bodies are incisional into sand-prone heterolithic deposits of F.A.2 and display transitional sedimentological features between the previously defined end-member types of elementary channel architectures (Fig. 10).

Higher in the stratigraphy, isolated, coarser-grained, strongly-confined channel elements and prominent channel complexes become embedded within, and markedly incisional into, a nearly 700 m thick succession of F.A.3 mud-prone heterolithic deposits (Figs. 4, 10). Here, chaotic slump deposits of facies LF 11, up to 2.5 m thick, have been locally documented. Isolated channel complexes, comprised of strongly-confined elements, are up to 45 m thick and are characterized by concave-upward, sharp erosional bases, longitudinally traceable for up to 3 km. Basal paleocurrent indicators reveal a main current flow directed toward S-SE (N 163), consistent with the regional dispersal pattern reported by Loiacono (1974) and Boiano (1997).

Interpretation. Isolated channel elements and channel complexes in the upper part of the GF succession have been interpreted by previous workers as large submarine slump deposits (Pescatore et al, 1980; Loiacono, 1993), produced by catastrophic avalanche processes induced by seismic shocks (Boiano, 1997; Giannandrea et al., 2016). However, the concave-up geometry of the extensive erosional bases and the internal facies distribution of these very coarse-grained sandbodies indicate a channelized nature.

The thick mud-prone heterolithic succession encasing the isolated channels (Fig. 10) can be interpreted to represent background slope deposits (e.g., Figueiredo et al., 2010; Bayliss and Pickering 2015b). Their formation is possibly related to two main causes: (i) a general shift of the turbidite system along the depositional profile; or (ii) an important phase of deactivation of the GF turbidite system, albeit with sporadic inputs of coarse-grained material allowing the development of isolated submarine channels. In this scenario, the configuration of the slope setting might be associated with a significant, tectonically-induced increase in the longitudinal gradient of the basin, as suggested by the presence of slump deposits (LF 11) within the mud-prone succession.

5.3. Channel planforms and stacking pattern

The spectacular exposures of the GF formation throughout the outcrop belt (Fig. 2) offer a unique opportunity for the reconstruction of the stratigraphic relationships between the main architectural units at the scale of the turbidite system. In particular, the analysis of the stacking pattern characterizing the channelized units is crucial to decipher the complex evolution of the GF formation in the study area and the role played by its main driving factors.

Submarine channel-belt architectures are typically dominated by the vertical aggradation of the channel-fill deposits, which record channel migration and document the repeated phases of infill and incision (e.g. Sylvester et al., 2011; Hodgson et al., 2011; Jobe et al., 2016). Stacking patterns dominated by vertical aggradation are usually developed in highly-confined channel systems with high rates of deposition (e.g. Labourdette and Bez, 2010; Janocko et al., 2013; Macauley and Hubbard, 2013) and the GF formation represents an excellent example of such systems.

The stacking architectures of the GF formation channelized units have been analyzed through the reconstruction of the channels' planform geometries (Fig. 11A). Major shifts in intra-element position (e.g., margin, off-axis or axis) were inferred from the channel-fill deposits within the CS 2 and the uppermost isolated channels/channel complexes, which are the best exposed units in the study area. The architectural data have been mapped and combined with paleoflow measurements from channel-fill deposits and heterolithic "out-of-channel" packages, allowing the progressive plan view reconstruction of the stacked channel deposits (Fig. 11A). Within the CS 2, six "time slices" have been considered to describe the variability of the large-scale planform geometries (Fig. 11A). These distinct moments in CS 2 evolution roughly correspond to the major extensive erosional surfaces identified at the base of CS 2A and within CS 2B, which define discrete channel complexes. The planform channel patterns so obtained show an overall low degree of sinuosity along the 13-km long outcrop belt. Furthermore, two additional time slices describe the planforms of isolated channels and channel complexes in the upper part of the GF succession, which exhibit a slightly higher degree of sinuosity than the CS 2 channel complexes, albeit maintaining a relatively straight trajectory (Fig. 11A).

Plan view reconstructions are used to project the inferred stacking trajectories of the GF channelized units in three-dimensions. A nearly E-W oriented cross-section, cutting the GF channels roughly perpendicular to the regional paleoflow direction, provides a representation of the general migration pattern and allows the stacking behavior of the channelized units to be analyzed (Fig. 11B). At the scale of the channel system, the CS 2 exhibits a marked aggradational architecture, revealed by its offset-stacked channel complexes. Their composite stacking pattern results from the migration of the channel system back and forth across the basin axis, initially directed towards W-SW and then back towards E-NE (Fig. 11B). This "zig-zag" migration pattern is recorded in the variable nature of the overbank deposits exposed between channel belts CS 2A and CS 2B, characterizing the central portion of the GF succession in the study area (Fig. 4). This extensive heterolithic package reaches a maximum thickness of approximately 400 m, pinching-out towards the N, where the CS 2A and CS 2B converge (Fig. 4). At the large scale, a clear fining- then coarsening-upward trend has been documented. This composite stratigraphic trend is interpreted to be related to the coupled lateral migration and aggradation through time of the channelized depocenter of the CS 2 (e.g., Schwarz and Arnott, 2007; Hubbard et al., 2009). Specifically, the large-scale fining-upward trend within the lower part of the heterolithic succession (i.e., from F.A.2 proximal overbank deposits above the CS 2A to F.A.3 distal overbank deposits) coincides with the combined aggradation and migration of the active part of the CS 2 towards the W-SW, away from the site of deposition of the overbank package. Conversely, the subsequent large-scale coarsening-upward trend in the upper part of the overbank succession (i.e., from distal F.A.3 to proximal F.A.2 deposits occurring directly beneath CS 2B) is interpreted to reflect the coupled aggradation and migration of the CS 2 back to the E-NE.

6. DISCUSSION

6.1. Effects of thrust tectonics on the stacking pattern

Channel complexes and complex sets forming prominent turbidite systems are commonly imaged in seismic reflection datasets acquired by the hydrocarbon industry. These systems are characterized by a composite stratigraphic architecture consisting of broad, laterally-stacked channel complex and complex-set fills at the base of the turbidite succession, followed by nearly vertically-aligned and aggradational channel complex and complex-set fills at the top (Sylvester et al., 2011; Jobe et al., 2016). This typical sequence of channel architectural styles records a multi-phase degradational-aggradational trend that has been documented globally in both seismic (e.g., Deptuck et al., 2003; Janocko et al., 2013, Covault et al., 2016) and outcrop (e.g., Brunt et al., 2013a; Hodgson et al., 2011; Macauley and Hubbard, 2013) datasets. In the GF succession, however, the initial laterally offset-stacked channel complexes and complex-sets comprising the lower portion of turbidite systems observed elsewhere has not been recognized. The entire CS 2 is instead characterized by a prominent aggradational nature combined with a limited lateral offset of its component channel complexes (Fig. 11B), resulting in a stacking pattern typically attributed to the late stages of channel complex-sets evolution (e.g., Myall et al., 2006; Bain and Hubbard, 2016).

The marked aggradational nature of the CS 2 is suggestive of significant creation of accommodation space (Clark and Cartwright, 2011; Hodgson et al., 2011). Within active foreland basin settings, such as the Southern Apennine foredeep, continuous creation of accommodation space might be a consequence of the subsidence related to subduction (Doglioni, 1991; 1994). Accommodation space in wedge-top depozones is commonly considered as the net result of competition between two main forces acting in the thrust-and-fold belt: the regional subsidence associated with subduction and the thrust-related fold uplift (i.e., the upward component of the thrust displacement; see Fig. 3 of Doglioni and Prosser, 1997). According to this process, when thrust-related folds rise at slower rates than the regional subsidence, net accommodation space is produced, allowing the channel system to aggrade. This particular tectonic setting is generally associated with orogenic belts, such as the Apennines, characterized by high rates of regional subsidence in the foredeep (up to 1600 m/M.y.)

due to the fast eastward rollback of the hinge of the W-dipping subduction zone (Mariotti and Doglioni, 2000).

The internal stacking architecture of the CS 2 can be interpreted to be governed by either autogenic or allogenic processes. Various mechanisms have been proposed to explain the migration trajectories commonly observed in submarine channel systems, including turbidity current flow properties (Kolla et al., 2007; Janocko et al., 2013), progressive levee growth (Peakall et al., 2000; Jobe et al., 2016), sediment supply versus accommodation (Kneller, 2003), changes in equilibrium profile (Hodgson et al., 2011) and effects of basin tectonics (Clark and Cartwright, 2009). However, the trigger for lateral channel migration is still poorly understood and many studies invoke complex interactions between these autogenic and allogenic processes (e.g. Hubbard et al., 2009; Di Celma et al., 2011; Thomas and Bodin, 2013). Among the different mechanisms that can be invoked, the activity of the regional thrust structures that configured a narrow turbidite basin might have played an important role in controlling the migration trajectories of the stacked channelised units in the CS 2. The observed migration pattern might have been influenced by the variable rate of growth of the internal, out-of-sequence thrust, which competed during its development with the ongoing subsidence of the basin (Fig. 12). This latter was associated to the progressive flexure of the underlying plate in the subduction zone and is assumed to have developed at constant rates during the evolution of the turbidite system. When the growth rate of the internal thrust was lower than the regional subsidence rate, the fast eastward roll-back in the subduction zone tilted the basin towards SW and likely determined the initial migration of the CS 2 depocenter towards W-SW (Fig. 12A). Conversely, when the thrust growth rate outpaced the regional subsidence rate, the channel system depocenter was progressively shifted towards E-NE, away from the axis of uplift of the thrust (Fig. 12B), in a process referred to as “deflection” (Clark and Cartwright, 2009; 2011).

A similar tectonically-induced, “zig-zag” migration pattern has been described by Hubbard et al. (2009) for the deep-water Tertiary channel system of the Puchkirchen and Hall formations in the Molasse foreland basin (Austria). There, active tectonic in the adjacent Alpine thrust-and-fold belt has been interpreted to have a direct impact on channel pattern and stacking behavior, shifting the axis of the whole channel system initially outward, away from the growing orogen (Hubbard et al., 2009). Then, the substantial deposition of a large overbank wedge on the external margin of the basin determined the switching of the migration direction of the channel system in the opposite direction (see Fig. 20 of Hubbard et al., 2009).

It is worth noting that the maximum lateral offset displayed by the major channelised units in the CS 2 is nearly 500 m (Fig. 11B), relatively limited if compared to the stacking patterns typically documented in other submarine channel systems worldwide (e.g., Hubbard et al., 2009; Sylvester et al., 2011; Bain and Hubbard, 2016). This limited lateral offset might be considered as an effect of the tectonically-induced narrow basin configuration. In general, a significant structural confinement imparted by the basin physiography tends to limit the ability of a channel system to migrate laterally, resulting in a restricted lateral stacking variability of the component channelized units, and thus preventing the large-scale avulsion of the channel belt (Hubbard et al., 2009; Labourdette and Bez, 2010). Accordingly, the reduced lateral space available within the narrow GF basin might have limited the lateral migration of the stacked channel complexes that form the CS 2 (Fig. 11B) and prevented the avulsion of the channel system in new positions.

The strong tectonic confinement of the GF channel system likely influenced the depositional architectures developed as heterolithic overbank packages flanking the channelized units in the CS 2. These overbank deposits commonly display an apparent tabular geometry at the outcrop scale. Although their effective tabularity cannot be consistently verified, due to limited exposure, this apparent feature might be related to the considerable width of overbank flows that spilled over the channel confinement. In this scenario, the low-density currents were probably basin-wide and constrained by the narrow basin width, which prevented the development of tapered levees (Saito and Ito, 2002; Takano et al., 2005). Many sand-rich submarine channel systems in relatively narrow basins are reported to have tabular overbank deposits instead of classical gull-wing-shaped levee ridges, as the deep-sea Toyama Trough (Sea of Japan), which is 30–40 km wide and >100 km long (Nakajima, 1996), and the Eocene Kusuri Formation in the Sinop Basin (Turkey), which is nearly 30 km wide and >150 km long (Janbu et al., 2009).

6.2. Stratigraphic evolution of the GF turbidite system

The reconstruction of the evolutionary history of an ancient turbidite system is one of the main goals of recent outcrop studies (e.g., Eschard et al., 2003; Pemberton et al., 2016). For this purpose, the accurate interpretation of the stratigraphic record and the analysis of spatial and temporal changes in depositional architectures are of primary importance (e.g., Mutti and Normark, 1987; Romans et al., 2011; Jobe et al., 2016). The robust dataset presented in this study shows that the nearly 2 km thick GF turbidite succession resulted from the complex interplay between the depositional processes controlling sand accumulation (i.e., weakly-confined channel fills vs strongly-confined channel fills) and the driving factors that governed the aggradation and stacking pattern of the deep-water channels (i.e., increasing subsidence, syn-sedimentary thrust tectonics structural basin confinement). At the scale of the turbidite system, the observed juxtaposition of different channel architectures and heterolithic deposits is interpreted to have been governed by the alternate in- and out-of-sequence tectonic pulses of the basin-bounding thrust structures, which controlled the coarse clastic inputs sourced from the orogenic hinterland. This overall change in depositional style likely reflects a varying position of the GF turbidite system along the paleo-depositional profile.

In submarine channel systems, a key control on flow properties and resulting architectural geometries of turbidite channels is commonly attributed to the submarine slope gradient (e.g., Wynn et al., 2002; Kneller, 2003), which may be modified by multiple factors, such as faulting, diapirism, sediment accretion, differential compaction, mass wasting (Prather, 2000) or tectonic tilting (McCaffrey et al., 2002; Ferry et al., 2005). Continued erosion or deposition may modify the slope profile, in relation to externally driven changes in volumes and frequencies of gravity flows (Cronin et al., 2000; Kneller, 2003).

The incisional nature of the amalgamated, strongly-confined channels of the CS 1, along with the presence of extraformational conglomerates (LF 1A) and flanking mud-prone overbank deposits (F.A.3), might suggest a likely initiation and development for these channels in a slope environment (e.g. Figueiredo et al., 2013; Bayliss and Pickering, 2015a), which presumably characterized the earlier phases of the GF basin evolution (Fig. 13A). The abundance of extraformational conglomerates reflects the protracted denudation of the source area, located to the W-NW in the orogenic hinterland (Critelli et al., 2017). High-energy sediment gravity-flows likely developed in response to increased gradients in the staging area, determined by the activity of the internal thrust structures of the Apennine thrust-and-fold belt that progressively uplifted the chain (Fig. 13A). The gradual de-activation of the sediment source area, possibly related to the decreasing rates of tectonic uplift in the SW and the concomitant early activation of the outer thrust to the NE, resulted in the filling and retrogradation of the slope environment after the deposition of the CS 1 (Fig. 13B). The deposition of the overlying, approximately 100 m thick interval of mud-prone heterolithic deposits (F.A.3) took place in this scenario (Figs. 7B, 12B). These deposits, characterized by very low sedimentation rates compared to the CS 1, might have recorded a substantial reduction of the seafloor gradient, favouring the establishment of a near base-of-slope setting. A similar stratigraphic trend, related to tectonically-induced variations of the seafloor gradient, has been documented in the Middle Eocene Morillo System (Ainsa basin, Spain) by Bayliss and Pickering (2015b).

After the initial phase of slope gradient readjustment, the deposition of the CS 2 took place, prompted by the re-activation of the internal, out-of-sequence regional thrust that restored the coarse clastic inputs in the turbidite basin from the western source area (Fig. 13C). This large channel complex-set comprises amalgamated, high aspect-ratio, weakly-confined channel elements, flanked by sand-prone overbank deposits (F.A.2). These particular types of channel architectures have been commonly documented in areas of low to moderate gradient on a paleo-depositional profile, in lower slope or base-of-slope settings, associated with strikingly sand-rich overbank deposits (e.g., Maier et al., 2011; Brunt et al., 2013b; Pemberton et al., 2016).

Higher up in the stratigraphy, amalgamated weakly-confined channels gradually evolve into isolated strongly-confined, low aspect-ratio channels, deeply incisional into the surrounding mudstones and very thin-bedded sandstones of F.A.3 (Fig. 13D). Evidence of protracted bypass of energetic gravity flows that commonly cut down for tens of meters into very fine-grained slope deposits are generally associated with middle- to upper-slope channels, commonly recognized in outcrops (e.g. Gardner et al., 2003; Hubbard et al., 2014) and seismic datasets (e.g., Mayall et al, 2006; Jobe et al., 2015).

In summary, the stratigraphic trend documented through the middle and upper portions of the GF succession, starting from the deposition of the CS 2, records a progressive increase of the slope gradient that resulted in a gradual increment in confinement of turbidity currents through time, as indicated by the stratigraphic transition from high aspect-ratio to low aspect-ratio channels (Prather, 2003; Pemberton et al., 2016). The increase of the slope-gradient is also marked by a progressive variation in the nature of the out-of-channel, heterolithic deposits upward in the stratigraphy, from sand-prone (F.A.2) to mud-prone (F.A.3). The overall upward change in sand content and channel architectural style is therefore interpreted to represent the progradation of a slope channel system (i.e., upper part of the GF succession) over a base-of-slope, weakly confined sand-prone channel system (i.e., the CS 2). This marked progradational trend developed during the late Miocene in association with the progressive infill of the narrow primary confinement (Fig. 13). Comparable progradational stratigraphic trends have been documented in different ancient turbidite systems, such as the Middle Eocene Banastón System in the Ainsa Basin of Spain (Bayliss and Pickering, 2015b) and the Unit B of the Permian Laingsburg Formation in the Karoo Basin of South Africa (Flint et al., 2011).

6.3 Reservoir Implications

Submarine channel systems are among the most important hydrocarbon clastic reservoirs currently being explored (e.g., Stewart et al., 2008; Covault et al., 2009; Reimchen et al., 2016). Outcropping turbidite successions have been investigated in great detail to improve the large-scale architectural characterization of analogous hydrocarbon-bearing units in the subsurface (e.g., Samuel et al., 2003; Beaubouef, 2004; Pyles et al., 2010). However, the lateral and vertical variability of most reservoir properties are associated with differences in the nature of channel fills and their related overbank deposits, which commonly are at scales below the resolution of even high-frequency 3D seismic (Mayall and Stewart 2000). Accordingly, the knowledge of the detailed distribution of sedimentary facies at the sub-seismic scale provides valuable insights into reservoir performance of the whole turbiditic system, aiding in the development of efficient production strategies (Beaubouef, 2004).

The multiple channelized units comprising the GF succession represent an ideal composite reservoir body, whose total thickness and lateral extension is comparable to those commonly imaged in seismic datasets (e.g., Kolla et al., 2001; Posamentier and Kolla, 2003; Myall et al., 2006). Moreover, it offers extensive exposures that allow detailed characterizations of the deep-water strata and therefore represents an important analogue for predicting and estimating the stratal architectures of channelized hydrocarbon-bearing reservoirs at multiple scales.

Individual channel elements in the GF system show predictable cross-sectional facies distribution. Both weakly-confined and strongly-confined channel-fill deposits display an excellent reservoir quality, with N:G between 0.9 and 1 (Fig. 4A). These deposits are dominated by thick-bedded, amalgamated structureless sandstones (LF 2) in the channel axis, with a general lack of fine-grained strata representing potential flow barriers. Within the channels, the lateral continuity of individual sandstone beds is highly variable because of the presence of internal erosional surfaces, commonly mantled by residual lags of facies LF 1. Matrix-supported extraformational conglomerates (LF 1A) and mudclast breccias (LF 1B) are also abundant above the channel bases and they could represent local low-permeability baffles to fluid flows and reduce the reservoir volume (e.g., Elliot, 2000; Navarro et al., 2007). However, the concentration of conglomerate clasts can be highly variable and therefore, in some locations, fluid flow is probably only marginally affected because of the good connectivity of the surrounding sandstone matrix. The reservoir quality diminishes (remaining nevertheless high) as the mean grain-size, bed thickness and degree of amalgamation decrease laterally towards the margins of the channels.

At the scale of channel complexes and complex sets, the reservoir connectivity and associated hydrocarbon recovery are strongly dependent on the stratigraphic relationships and stacking patterns of the different channelized units (Funk et al., 2012; Reimchen et al., 2016). Fluid flow behavior during hydrocarbon production is likely to vary according to the large-scale reservoir architecture that differs as a function of the incising to aggrading trajectory of a channel system (Covault et al., 2016).

In the case of the GF formation, the CS 2 represents a prominent continuous reservoir, due to its considerable thickness and extension (Fig. 4), with vertically connected sandstone-rich facies. The component channel complexes stack aggradationally, with limited lateral offset (Fig 12B), and therefore suggest good vertical reservoir communication within the channel-complex set (Pyles et al., 2010; Funk et al., 2012). Reservoir quality degrades from the axis toward the channel complex-set margins, in relation to the lateral transition from amalgamated channel-fill deposits to laterally-persistent lenticular sandbodies, exposed in the southern sector of the CS 2B (Fig. 4). Despite the high sandstone content of these marginal strata, their architectural configuration, characterized by a comparative minor thickness (average 14 m) and limited lateral extent, increase the potential reservoir compartmentalization at the system scale. The stacked weakly-confined channels forming the CS 2 are laterally-associated with sand-prone proximal overbank deposits of F.A.2 (Fig. 4). Their reservoir quality is good (N:G between 0.65 and 0.85; Fig. 4B), owing to the presence of well-sorted sandstones (facies LF 5 to 10). These facies are characterized by high permeability, but porosity values slightly lower than those of channel-fill deposits, due to their comparatively lower grain-size (Hansen et al., 2015). Their predominantly tabular geometry promotes lateral migration of fluids. However, the vertical permeability within F.A.2 packages is very low, due to the rare amalgamations between the sandstone beds, which are interbedded with extensive thin mudstone intervals. Sand-prone overbank packages are locally truncated by weakly-confined channel-fill deposits, forming sand-on-sand contacts along the erosional channel bases. These contacts considerably improve reservoir connectivity and increase the potential reservoir volume, making it possible to produce fluids from channels and overbank deposits simultaneously (Navarro et al., 2007; Funk et al., 2012).

On the other hand, the basal CS 1 and the isolated channels and channel complexes in the upper part of the GF succession might be considered as isolated compartments of the reservoir system, due to their stratigraphic position without any sand or gravel connection with the CS 2. CS 1 and the upper isolated channels are flanked and overlain by mud-prone heterolithic deposits of F.A.3 (Figs. 4, 7). These thick heterolithic packages are characterized by low N:G values, between 0.1 and 0.4 (Fig. 4C), and can be considered as barriers to fluid flows, in relation to the presence of thick, laterally continuous mudstone intervals. However, the coarse-grained shallow scour-fill deposits (LF 5) that locally occur within the mud-prone succession potentially represent good reservoir units, albeit with limited lateral extension and lenticular geometry.

7. CONCLUSIONS

The deep-water strata of the Gorgoglione Flysch (GF) Formation document a protracted history of sediment transfer and deposition through a long-lived channel system, developed during the late Miocene in a narrow and elongated thrust-top basin of the Southern Apennines (Italy). A wide range of erosional and depositional processes is recorded in an exceptionally-preserved outcrop belt, oriented sub-parallel to the basin axis and regional paleoflow. The spectacular exposures of the GF succession provide a rare opportunity to characterize the spatio-temporal evolution of a submarine channel system at a scale similar to that commonly imaged on seismic datasets, but with the stratigraphic detail exclusive of outcrop studies.

Channel-fill facies, including matrix-supported extraformational conglomerates, mudclast-rich conglomerates and coarse-grained sandstones, are laterally juxtaposed against sand-prone and mud-prone, out-of-channel heterolithic deposits. Across the study area, channel-fill deposits display variable depositional features that have been associated with two end-member types of elementary channel architectures: high aspect-ratio, weakly-confined channels and low aspect-ratio, strongly-confined channels. Their stratigraphic distribution throughout the GF succession deeply controls the seismic-scale depositional style of the main architectural units developed in the turbidite system, together with their reservoir-scale heterogeneity. From the base of the succession, two discrete channel complex-sets have been recognized, separated by an approximately 100 m thick package of heterolithic slope deposits (Fig. 13B): (1) the CS 1, which is isolated in the lowermost portion of the GF succession and is composed of amalgamated strongly-confined channels, laterally associated with mud-prone overbank deposits; and (2) the CS 2, which is exposed extensively throughout the study area and represents nearly the 80% of the gross channel system sandstones. This prominent channel complex set, comprised of amalgamated weakly-confined channels flanked by heterolithic overbank deposits of F.A.2 and F.A.3, exhibits a markedly aggradational stacking pattern with a limited lateral offset of its component channel complexes. Above the CS 2, isolated channels and channel complexes occur, consisting of strongly-confined elementary channels embedded within, and considerably incisional into, mud-prone heterolithic slope deposits.

The observed sequence of channelized architectural units is interpreted to have been governed at multiple scales by the thrust tectonics of the Southern Apennines, in combination with a high subsidence rate that promoted significant aggradation. The alternate in- and out-of-sequence tectonic pulses of the thrust structures delimiting the GF basin controlled the activation of the coarse-clastic inputs and the resulting stacking architectures of the channelised units. The tectonic confinement of the depositional system resulted in a narrow basin morphology and possibly limited the lateral offset in channel stacking documented in the CS 2, preventing large-scale avulsions. Moreover, the confinement might have favored the tabular depositional geometries of the heterolithic overbank deposits associated with the channel-fill successions.

The overall change in depositional style, revealed by the marked juxtaposition of different channel architectures and heterolithic deposits, allowed the temporal and spatial evolution of the GF system to be reconstructed. The general stratigraphic trend likely reflects a varying position of the GF turbidite system along the paleo-depositional profile. In particular, the overall upward change in sand content and channel architectures, expressed in the gradual stratigraphic transition from the CS 2 to the upper isolated channels, is interpreted to record the general progradation of a slope channel system over a near base-of-slope channel system.

In conclusion, examination of the GF turbidite succession highlights the key architectural and sedimentological features typical of channel systems developed within confined and elongate basins, supporting the development of a well-constrained predictive model for reservoir-sandstone distribution that can be translated to analogous depositional systems in the subsurface. The comprehensive dataset presented from the northern sector of the GF basin represents a rare case study from outcrop of depositional and erosional processes in a confined base-of-slope to slope setting. The results of this study should find wide applicability in other basins, particularly those that formed in strongly active tectonic settings. The documented depositional styles, scale of the component architectural units, and stacking patterns of the sandbodies provide useful comparisons with hydrocarbon reservoirs where important tectonic structures have controlled the sedimentation.

REFERENCES

Allen, J.R. (1963). The classification of cross-stratified units with notes on their origin. Sedimentology, 2(2), 93-114.

Arnott, R.W.C., Navarro, L., & Khan, Z.A. (2011). Contrasting the stratal architecture of highly-confined and poorly-confined deep-marine sinuous channel systems – an outcrop perspective. In: Mayall, M., Kane, I., McCaffrey, W. D., eds., Internal architecture, bedforms and geometry of turbidite channels, The geological Society of London, June 20-21, 2011.

Babonneau, N., Savoye, B., Cremer, M., & Bez, M. (2010). Sedimentary architecture in meanders of a submarine channel: detailed study of the present Congo turbidite channel (Zaiango project). Journal of Sedimentary Research, 80(10), 852-866.

Bain, H.A., & Hubbard, S.M. (2016). Stratigraphic evolution of a long-lived submarine channel system in the Late Cretaceous Nanaimo Group, British Columbia, Canada. Sedimentary Geology, 337, 113-132.

Barton, M., O'Byrne, C., Pirmez, C., Prather, B., Van der Vlugt, F., Alpak, F.O., & Sylvester, Z. (2010). Turbidite channel architecture: Recognizing and quantifying the distribution of channel-base drapes using core and dipmeter data. In: Pöppelreiter, M., García-Carballido, C., Kraaijveld, M.A., eds., Dipmeter and Borehole Image Log Technology. AAPG Memoir 92, pp. 195–210.

Bayliss, N.J., & Pickering, K.T. (2015 a). Transition from deep-marine lower-slope erosional channels to proximal basin-floor stacked channel–levée–overbank deposits, and syn-sedimentary growth structures, Middle Eocene Banastón System, Ainsa Basin, Spanish Pyrenees. Earth-Science Reviews, 144, 23-46.

Bayliss, N.J., & Pickering, K.T. (2015 b). Deep-marine structurally confined channelized sandy fans: Middle Eocene Morillo System, Ainsa Basin, Spanish Pyrenees. Earth-Science Reviews, 144, 82-106.

Beaubouef, R.T. (2004). Deep-water leveed-channel complexes of the Cerro Toro Formation, Upper Cretaceous, southern Chile. AAPG Bulletin, 88(11), 1471-1500.

Beaubouef, R.T., Rossen, C., Zelt, F.B., Sullivan, M.D., Mohrig, D.C., & Jennette, D.C. (1999). Deep-water sandstones, Brushy Canyon Formation, west Texas. Field guide for American Association of Petroleum Geologists, Hedberg Field Research Conference. AAPG Continuing Education Course Note Series 40, p. 47.

Boiano, U. (1997). Anatomy of a siliciclastic turbidite basin: the Gorgoglione Flysch, Upper Miocene, southern Italy: physical stratigraphy, sedimentology and sequence-stratigraphic framework. Sedimentary Geology, 107(3), 231-262.

Bouma, A.H. (1962). Sedimentology of Some Flysch Deposits; A Graphic Approach to Facies Interpretation: Amsterdam, Elsevier, 168 pp.

Brunt, R.L., & McCaffrey, W.D. (2007). Heterogeneity of fill within an incised channel: The Oligocene Gres du Champsaur, SE France. Marine and Petroleum Geology, 24(6), 529-539.

Brunt, R.L., Di Celma, C.N., Hodgson, D.M., Flint, S.S., Kavanagh, J.P., van der Merwe, W.C. (2013 a). Driving a channel through a levee when the levee is high: An outcrop example of submarine down-dip entrenchment. Marine and Petroleum Geology, 41, 134-145.

Brunt, R.L., Hodgson, D.M., Flint, S.S., Pringle, J.K., Di Celma, C., Prélat, A., & Grecula, M. (2013 b). Confined to unconfined: anatomy of a base of slope succession, Karoo Basin, South Africa. Marine and Petroleum Geology, 41, 206-221.

Butler, R.W., & Tavarnelli, E. (2006). The structure and kinematics of substrate entrainment into high-concentration sandy turbidites: a field example from the Gorgoglione 'flysch' of southern Italy. Sedimentology, 53(3), 655-670.

Camacho, H., Busby, C.J., & Kneller, B. (2002). A new depositional model for the classical turbidite locality at San Clemente State Beach, California. AAPG Bulletin, 86(9), 1543-1560.

Campion, K.M., Sprague, A.R. & Sullivan, M.D. (2005). Architecture and Lithofacies of the Capistrano Formation (Miocene-Pliocene), San Clemente, California. The Pacific Section SEPM, 42 p.

Cavalcante, F., Prosser, G., Agosta, F., Belviso, C., & Corrado, G. (2015). Post-depositional history of the Miocene Gorgoglione Formation (southern Apennines, Italy): inferences from mineralogical and structural analyzes. Bulletin de la Société Géologique de France, 186(4-5), 243-256.

Clark, I.R., & Cartwright, J.A. (2009). Interactions between submarine channel systems and deformation in deep-water fold belts: Examples from the Levant Basin, Eastern Mediterranean Sea. Marine and Petroleum Geology, 26(8), 1465-1482.

Clark, I.R., & Cartwright, J.A. (2011). Key controls on submarine channel development in structurally active settings. Marine and Petroleum Geology, 28(7), 1333-1349.

Clark, J.D., & Pickering, K.T. (1996). Architectural elements and growth patterns of submarine channels: application to hydrocarbon exploration. AAPG Bulletin, 80(2), 194-220.

Covault, J.A., Hubbard, S.M., Graham, S.A., Hinsch, R., & Linzer, H.G. (2009). Turbidite-reservoir architecture in complex foredeep-margin and wedge-top depocenters, Tertiary Molasse foreland basin system, Austria. Marine and Petroleum Geology, 26(3), 379-396.

Covault, J.A., Sylvester, Z., Hubbard, S.M., Jobe, Z.R., Sech, R.P. (2016). The stratigraphic record of submarine – channel evolution. The Sedimentary Record, 14, 4-11.

Critelli, S. & Loiacono, F. (1988). Provenienza e dispersione dei sedimenti nel flysch di Gorgoglione (Langhiano–Tortoniano, Appennino Lucano): Implicazioni sull'evoluzione delle mode detritiche arenacee nell'orogene sudappenninico. Mem. Soc. Geol. It. 41, 809-826.

Critelli, S., Muto, F., Perri, F., & Tripodi, V. (2017). Interpreting provenance relations from sandstone detrital modes, southern Italy foreland region: Stratigraphic record of the Miocene tectonic evolution. Marine and Petroleum Geology.

Cronin, B.T., Hartley, A.J., Celik, H., Hurst, A., Turkmen, I., & Kerey, E. (2000). Equilibrium profile development in graded deep-water slopes: Eocene, Eastern Turkey. Journal of the Geological Society, 157(5), 943-955.

Deptuck, M.E., Steffens, G.S., Barton, M., & Pirmez, C. (2003). Architecture and evolution of upper fan channel-belts on the Niger Delta slope and in the Arabian Sea. Marine and Petroleum Geology, 20(6), 649-676.

Di Celma, C.N., Brunt, R.L., Hodgson, D.M., Flint, S.S., & Kavanagh, J.P. (2011). Spatial and temporal evolution of a Permian submarine slope channel–levee system, Karoo Basin, South Africa. Journal of Sedimentary Research,81(8), 579-599.

Doglioni, C. (1991). A proposal for the kinematic modelling of W-dipping subductions; possible applications to the Tyrrhenian-Apennines system. Terra Nova, 3, 423-434.

Doglioni, C. (1994). Foredeeps versus subduction zones. Geology, 22(3), 271-274.

Doglioni, C., & Prosser, G. (1997). Fold uplift versus regional subsidence and sedimentation rate. Marine and Petroleum Geology, 14(2), 179-190.

Elliott, T. (2000). Depositional architecture of a sand-rich, channelized turbidite system: the Upper Carboniferous Ross Sandstone Formation, western Ireland. In: Weimer, P., et al., eds., Turbidite Reservoirs of the World. 20th Annual Gulf Coast Section SEPM Proceedings, pp. 342–373.

Eschard, R., Albouy, E., Deschamps, R., Euzen, T., & Ayub, A. (2003). Downstream evolution of turbidite channel complexes in the Pab Range outcrops (Maastrichtian, Pakistan). Marine and Petroleum Geology, 20, 691–710.

Etienne, S., Mulder, T., Bez, M., Desaubliaux, G., Kwasniewski, A., Parize, O., Dujoncquoy, E., & Salles, T. (2012). Multiple scale characterization of sand-rich distal lobe deposit variability: examples from the Annot Sandstones Formation, Eocene–Oligocene, SE France. Sedimentary Geology, 273, 1-18.

Ferry, J.N., Mulder, T., Parize, O., & Raillard, S. (2005). Concept of equilibrium profile in deep-water turbidite system: effects of local physiographic changes on the nature of sedimentary process and the geometries of deposits. Geological Society, London, Special Publications, 244(1), 181-193.

Figueiredo, J.J., Hodgson, D.M., Flint, S.S., & Kavanagh, J.P. (2010). Depositional environments and sequence stratigraphy of an exhumed Permian mudstone-dominated submarine slope succession, Karoo Basin, South Africa.Journal of Sedimentary Research, 80(1), 97-118.

Figueiredo, J.J., Hodgson, D.M., Flint, S.S., & Kavanagh, J.P. (2013). Architecture of a channel complex formed and filled during long-term degradation and entrenchment on the upper submarine slope, Unit F, Fort Brown Fm., SW Karoo Basin, South Africa. Marine and Petroleum Geology, 41, 104-116.

Flint, S.A., Hodgson, D.M., Sprague, A.R., Brunt, R.L., Van der Merwe, W.C., Figueiredo, J., Prelat, A., Box, D., Di Celma, C., & Kavanagh, J. P. (2011). Depositional architecture and sequence stratigraphy of the Karoo basin floor to shelf edge succession, Laingsburg depocenter, South Africa. Marine and Petroleum Geology, 28(3), 658-674.

Funk, J.E., Slatt, R.M., & Pyles, D.R. (2012). Quantification of static connectivity between deep-water channels and stratigraphically adjacent architectural elements using outcrop analogs. AAPG Bulletin, 96(2), 277-300.

Gardner, M.H., & Borer, J.M. (2000). Submarine channel architecture along a slope to basin profile, Brushy Canyon Formation, west Texas. Special Publications SEPM, 68, 195-214.

Gardner, M.H., Borer, J.M., Melick, J.J., Mavilla, N., Dechesne, M., & Wagerle, R.N. (2003). Stratigraphic process-response model for submarine channels and related features from studies of Permian Brushy Canyon outcrops, West Texas. Marine and Petroleum Geology, 20(6), 757-787.

Ghosh, B., & Lowe, D.R. (1993). The architecture of deep-water channel complexes, Cretaceous Venado sandstone member, Sacramento Valley, California. In: Advances in the Sedimentary Geology of the Great Valley Group, Sacramento Valley, California, (Eds S.A. Graham and D.R. Lowe), SEPM, Pacific Section, Guidebook 73, 51–65.

Giannandrea, P., Loiacono, F., Maiorano, P., Lirer, F., & Puglisi, D. (2016). Geological map of the eastern sector of the Gorgoglione Basin (southern Italy). Italian Journal of Geosciences, 135(1), 120-141.

Grundvåg, S.A., Johannessen, E.P., Helland-Hansen, W., & Plink-Björklund, P. (2014). Depositional architecture and evolution of progradationally stacked lobe complexes in the Eocene Central Basin of Spitsbergen. Sedimentology, 61(2), 535-569.

Gueguen, E., Doglioni, C., & Fernandez, M. (1998). On the post-25 Ma geodynamic evolution of the western Mediterranean. Tectonophysics, 298(1), 259-269.

Hansen, L.A., Callow, R.H., Kane, I. A., Gamberi, F., Rovere, M., Cronin, B.T., & Kneller, B.C. (2015). Genesis and character of thin-bedded turbidites associated with submarine channels. Marine and Petroleum Geology, 67, 852-879.

Hiscott, R.N., Hall, F.R., & Pirmez, C. (1997). Turbidity-current overspill from the Amazon Channel: texture of the silt/sand load, paleoflow from anisotropy of magnetic susceptibility, and implications for flow processes. In: Proceedings - ocean drilling program scientific results, National Science Foundation, pp. 53-78.

Hodgson, D.M., Di Celma, C.N., Brunt, R.L., & Flint, S.S. (2011). Submarine slope degradation and aggradation and the stratigraphic evolution of channel–levee systems. Journal of the Geological Society, 168(3), 625-628.

Hubbard, S.M., de Ruig, M.J., & Graham, S.A. (2009). Confined channel-levee complex development in an elongate depo-center: deep-water Tertiary strata of the Austrian Molasse basin. Marine and Petroleum Geology, 26(1), 85-112.

Hubbard, S.M., Covault, J.A., Fildani, A., & Romans, B.W. (2014). Sediment transfer and deposition in slope channels: deciphering the record of enigmatic deep-sea processes from outcrop. Geological Society of America Bulletin, 126(5-6), 857-871.

Janbu, N.E., Nemec, W., & Kirman, E. (2009). Facies Anatomy of a Sand-Rich Channelized Turbiditic System: The Eocene Kusuri Formation in the Sinop Basin, North-Central Turkey. Sedimentary Processes, Environments and Basins: A Tribute to Peter Friend, 457-517.

Janocko, M., Nemec, W., Henriksen, S., & Warchoł, M. (2013). The diversity of deep-water sinuous channel belts and slope valley-fill complexes. Marine and Petroleum Geology, 41, 7-34.

Jobe, Z.R., Howes, N.C., & Auchter, N.C. (2016). Comparing submarine and fluvial channel kinematics: Implications for stratigraphic architecture. Geology, G38158-1.

Kane, I.A., Kneller, B.C., Dykstra, M., Kassem, A., & McCaffrey, W.D. (2007). Anatomy of a submarine channel–levee: an example from Upper Cretaceous slope sediments, Rosario Formation, Baja California, Mexico.Marine and Petroleum Geology, 24(6), 540-563.

Kane, I.A., Dykstra, M.L., Kneller, B.C., Tremblay, S., & McCaffrey, W.D. (2009). Architecture of a coarse-grained channel–levée system: the Rosario Formation, Baja California, Mexico. Sedimentology, 56(7), 2207-2234.

Kane, I.A., & Hodgson, D.M. (2011). Sedimentological criteria to differentiate submarine channel levee subenvironments: exhumed examples from the Rosario Fm. (Upper Cretaceous) of Baja California, Mexico, and the Fort Brown Fm.(Permian), Karoo basin, S. Africa. Marine and Petroleum Geology, 28(3), 807-823.

Kneller, B. (2003). The influence of flow parameters on turbidite slope channel architecture. Marine and Petroleum Geology, 20(6), 901-910.

Kneller, B.C., & McCaffrey, W.D. (2003). The interpretation of vertical sequences in turbidite beds: the influence of longitudinal flow structure. Journal of Sedimentary Research, 73(5), 706-713.

Kolla, V., Bourges, P., Urruty, J.M., & Safa, P. (2001). Evolution of deep-water Tertiary sinuous channels offshore Angola (west Africa) and implications for reservoir architecture. AAPG Bulletin, 85(8), 1373-1405.

Kolla, V., Posamentier, H.W., & Wood, L.J. (2007). Deep-water and fluvial sinuous channels—Characteristics, similarities and dissimilarities, and modes of formation. Marine and Petroleum Geology, 24(6), 388-405.

Labourdette, R., & Bez, M. (2010). Element migration in turbidite systems: Random or systematic depositional processes? AAPG Bulletin, 94(3), 345-368.

Larue, D.K., & Provine, K.G. (1988). Vacillatory turbidites, Barbados. Sedimentary Geology, 57(3-4), 211-219.

Li, P., Kneller, B.C., Hansen, L., & Kane, I.A. (2016). The classical turbidite outcrop at San Clemente, California revisited: An example of sandy submarine channels with asymmetric facies architecture. Sedimentary Geology, 346, 1-16.

Loiacono, F. (1974). Osservazioni sulla direzione delle paleocorrenti nel Flysch di Gorgoglione (Lucania). Bollettino della Società Geologica Italiana, 93: 1127-1155.

Loiacono, F. (1993). Geometrie e caratteri deposizionali dei corpi arenacei nella successione stratigrafica del Flysch di Gorgoglione (Miocene sup., Appennino meridionale). Bollettino della Società Geologica Italiana, 112: 909-922.

Lowe, D.R. (1982). Sediment gravity flows: II. Depositional models with special reference to the deposits of high-density turbidity currents. Journal of Sedimentary Petrology, 52, 279 – 297.

Macauley, R.V., & Hubbard, S.M. (2013). Slope channel sedimentary processes and stratigraphic stacking, Cretaceous Tres Pasos Formation slope system, Chilean Patagonia. Marine and Petroleum Geology, 41, 146-162.

Maier, K.L., Fildani, A., Paull, C.K., Graham, S.A., McHargue, T.R., Caress, D.W., & McGann, M. (2011). The elusive character of discontinuous deep-water channels: New insights from Lucia Chica channel system, offshore California. Geology, 39(4), 327-330.

Mariotti, G., & Doglioni, C. (2000). The dip of the foreland monocline in the Alps and Apennines. Earth and Planetary Science Letters, 181(1), 191-202.

Mayall, M., & Stewart, I. (2000). The architecture of turbidite slope channels. In Deep-Water Reservoirs of the World: SEPM, Gulf Coast Section, 20th Annual Research Conference (Vol. 578, p. 586).

Mayall, M., Jones, E., & Casey, M. (2006). Turbidite channel reservoirs—Key elements in facies prediction and effective development. Marine and Petroleum Geology, 23(8), 821-841.

McCaffrey, W.D., Gupta, S., & Brunt, R. (2002). Repeated cycles of submarine channel incision, infill and transition to sheet sandstone development in the Alpine Foreland Basin, SE France. Sedimentology, 49(3), 623-635.

McCaffrey, W.D., & Kneller, B.C. (2004). Scale effects of non-uniformity on deposition from turbidity currents with reference to the Gres d'Annot of SE France. Geological Society, London, Special Publications, 221(1), 301-310.

McHargue, T., Pyrcz, M.J., Sullivan, M.D., Clark, J.D., Fildani, A., Romans, B.W., Covault, J.A., Levy, M., Posamentier, H.W. & Drinkwater, N.J. (2011). Architecture of turbidite channel systems on the continental slope: Patterns and predictions. Marine and Petroleum Geology 28(3): 728-743.

Migeon, S., Mulder, T., Savoye, B., & Sage, F. (2012). Hydrodynamic processes, velocity structure and stratification in natural turbidity currents: results inferred from field data in the Var Turbidite System. Sedimentary Geology, 245, 48-62.

Mutti, E. (1992). Turbidite sandstones. Agip, Istituto di geologia, Università di Parma.

Mutti, E., & Normark, W.R. (1987). Comparing examples of modern and ancient turbidite systems: problems and concepts. In: J.K. Leggett and G.G. Zuffa (Eds), Marine Clastic Sedimentology. Graham and Trotman, London, pp. I-38.

Nakajima, T. (1996). Turbidite sedimentation along the Toyama deep-sea channel in the Japan Sea. Unpublished Doctoral Thesis, Kyoto University, 108 pp.

Navarro, L., Khan, Z., & Arnott R.W.C. (2007). Depositional architecture and evolution of a deep-marine channel-levee complex: Isaac Formation (Windermere Supergroup), Southern Canadian Cordillera. In: T. H. Nilsen, R. D. Shew, G. S. Steffens, and J. R. J. Studlick, eds., Atlas of deep-water outcrops: AAPG Studies in Geology 56, CD-ROM, 22 p.

Patacca, E., & Scandone, P. (2007). Geology of the Southern Apennines. In Mazzotti, A., Patacca, E., and Scandone, P., eds., Results of the CROP Project, Sub-project CROP 04 Southern Apennines (Italy): Bollettino della Società Geologica Italiana (Italian Journal of Geoscience), Special Issue no. 7, 75–119.

Patacci, M. (2016). A high-precision Jacob's staff with improved spatial accuracy and laser sighting capability. Sedimentary Geology, 335, 66-69.

Peakall, J., McCaffrey, W.D., & Kneller, B.C. (2000). A process model for the evolution, morphology, and architecture of sinuous submarine channels. Journal of Sedimentary Research 70(3): 434-448.

Peakall, J., & Sumner, E.J. (2015). Submarine channel flow processes and deposits: A process-product perspective. Geomorphology, 244, 95-120.

Pescatore, T., Salvati, G., & Tramutoli, M. (1980). Regressive depositional cycles in the Gorgoglione flysch, Irpinids (Southern Italy). Geologica Romana, 19, 51-61.

Piedilato, S., & Prosser, G. (2005). Thrust sequences and evolution of the external sector of a fold and thrust belt: an example from the Southern Apennines (Italy). Journal of Geodynamics, 39(4), 386-402.

Pirmez, C., Beaubouef, R.T., Friedmann, S.J., & Mohrig, D.C. (2000). Equilibrium profile and baselevel in submarine channels: examples from Late Pleistocene systems and implications for the architecture of deep-water reservoirs. In Global deep-water reservoirs: Gulf Coast Section SEPM Foundation 20th Annual Bob F. Perkins Research Conference (pp. 782-805).

Pitts, A., Casciano, C.I., Patacci, M., Longhitano, S.G., Di Celma, C., & McCaffrey, W.D., (2017). Integrating traditional field methods with emerging digital techniques for enhanced outcrop analysis of deep-water channel-fill deposits. Marine and Petroleum Geology special issue: Sedimentology in Italy: recent advances and insights.

Porter, M.L., Sprague, A.R.G., Sullivan, M.D., Jennette, D.C., Beaubouef, R.T., Garfield, T.R., Rossen, C., Sickafoose, D.K., Jensen, G.N., Friedmann, S.J., & Mohrig, D.C. (2006). Stratigraphic organization and predictability of mixed coarse- and fine-grained lithofacies successions in a lower Miocene deep-water slope-channel system, Angola Block 15. In P.M. Harris and L.J. Weber, eds., Giant hydrocarbon reservoirs of the world: From Rocks to reservoir characterization and modeling: AAPG Memoir 88/SEPM Special Publication, p. 281–305.

Posamentier, H.W., & Kolla, V. (2003). Seismic geomorphology and stratigraphy of depositional elements in deep-water settings. Journal of Sedimentary Research, 73(3), 367-388.

Prather, B.E. (2000). Calibration and visualization of depositional process models for above-grade slopes: a case study from the Gulf of Mexico. Marine and Petroleum Geology, 17(5), 619-638.

Prélat, A., Hodgson, D.M., & Flint, S.S. (2009). Evolution, architecture and hierarchy of distributary deep-water deposits: a high-resolution outcrop investigation from the Permian Karoo Basin, South Africa. Sedimentology, 56(7), 2132-2154.

Pyles, D.R., Jennette, D.C., Tomasso, M., Beaubouef, R.T., & Rossen, C. (2010). Concepts learned from a 3D outcrop of a sinuous slope channel complex; Beacon Channel Complex, Brushy Canyon Formation, West Texas, U.S.A. Journal of Sedimentary Research 80(1-2): 67-96.

Reimchen, A.P., Hubbard, S.M., Stright, L., & Romans, B.W. (2016). Using sea-floor morphometrics to constrain stratigraphic models of sinuous submarine channel systems. Marine and Petroleum Geology, 77, 92-115.

Romans, B.W., Fildani, A., Hubbard, S.M., Covault, J.A., Fosdick, J.C., & Graham, S.A. (2011). Evolution of deep-water stratigraphic architecture, Magallanes Basin, Chile. Marine and Petroleum Geology, 28(3), 612-628.

Saito, T., & Ito, M. (2002). Deposition of sheet-like turbidite packets and migration of channel-overbank systems on a sandy submarine fan: an example from the Late Miocene–Early Pliocene forearc basin, Boso Peninsula, Japan. Sedimentary Geology, 149(4), 265-277.

Samuel, A., Kneller, B., Raslan, S., Sharp, A., & Parsons, C. (2003). Prolific deep-marine slope channels of the Nile Delta, Egypt. AAPG Bulletin, 87(4), 541-560.

Schwarz, E., & Arnott, R.W.C. (2007). Anatomy and evolution of a slope channel-complex set (Neoproterozoic Isaac Formation, Windermere Supergroup, southern Canadian Cordillera): implications for reservoir characterization. Journal of Sedimentary Research, 77(2), 89-109.

Sprague, A.R.G., Garfield, T.R., Goulding, F.J., Beaubouef, R.T., Sullivan, M.D., Rossen, C., Campion, K.M., Sickafoose, D.K., Abreu, V., Schellpeper, M.E., Jensen, G.N., Jennette, D.C., Pirmez, C., Dixon, B. T., Ying, D., Ardill, J., Mohrig, D.C., Porter, M.L., Farrell, M.E., & Mellere, D. (2005). Integrated Slope Channel Depositional Models: The Key to Successful Prediction of Reservoir Presence and Quality in Offshore West Africa. In: CIPM - E-Exitep 2005, Feb 20-23, 2005, Veracruz, México. 1-13.

Stevenson, C.J., Jackson, C.A.L., Hodgson, D.M., Hubbard, S.M., & Eggenhuisen, J.T. (2015). Deep-water sediment bypass. Journal of Sedimentary Research, 85(9), 1058-1081.

Stewart, J., Dunn, P.A., Lyttle, C., Campion, K., Oyerinde, A., & Fischer, B. (2008, January). Improving Performance Prediction in Deep-Water Reservoirs: Learning from Outcrop Analogues, Conceptual Models and Flow Simulation. In International Petroleum Technology Conference. International Petroleum Technology Conference.

Stright, L., Stewart, J., Campion, K., & Graham, S. (2014). Geologic and seismic modeling of a coarse-grained deep-water channel reservoir analog (Blacks Beach, La Jolla, California). AAPG Bulletin, 98(4), 695-728.

Sylvester, Z., Pirmez, C., & Cantelli, A. (2011). A model of submarine channel-levee evolution based on channel trajectories: Implications for stratigraphic architecture. Marine and Petroleum Geology, 28(3), 716-727.

Sylvester, Z., & Covault, J.A. (2016). Development of cutoff-related knickpoints during early evolution of submarine channels. Geology, 44(10), 835-838.

Takano, O., Tateishi, M., & Endo, M. (2005). Tectonic controls of a backarc trough-fill turbidite system: The Pliocene Tamugigawa Formation in the Niigata–Shin'etsu inverted rift basin, Northern Fossa Magna, central Japan.Sedimentary Geology, 176(3), 247-279.

Talling, P.J., Masson, D.G., Sumner, E.J., & Malgesini, G. (2012). Subaqueous sediment density flows: depositional processes and deposit types. Sedimentology, 59(7), 1937-2003.

Thomas, M.F.H., & Bodin, S. (2013). Architecture and evolution of the Finale channel system, the Numidian Flysch Formation of Sicily; insights from a hierarchical approach. Marine and Petroleum Geology, 41, 163-185.

Van der Merwe, W.C., Hodgson, D.M., Brunt, R.L., & Flint, S.S. (2014). Depositional architecture of sand-attached and sand-detached channel-lobe transition zones on an exhumed stepped slope mapped over a 2500 km2 area. Geosphere, 10(6), 1076-1093.

Vezzani, L., Festa, A., & Ghisetti, F.C. (2010). Geology and Tectonic Evolution of the Central-Southern Apennines, Italy: Geological Society of America Special Papers, 469, 1- 58.

Walker, R.G. (1984). Turbidites and associated coarse clastic deposits. In: Facies models (Vol. 1, pp. 171-188). Ontário: Geological Association of Canada.

Wynn, R.B., Kenyon, N.H., Masson, D.G., Stow, D.A., & Weaver, P.P. (2002). Characterization and recognition of deep-water channel-lobe transition zones. AAPG Bulletin, 86(8).

FIGURES

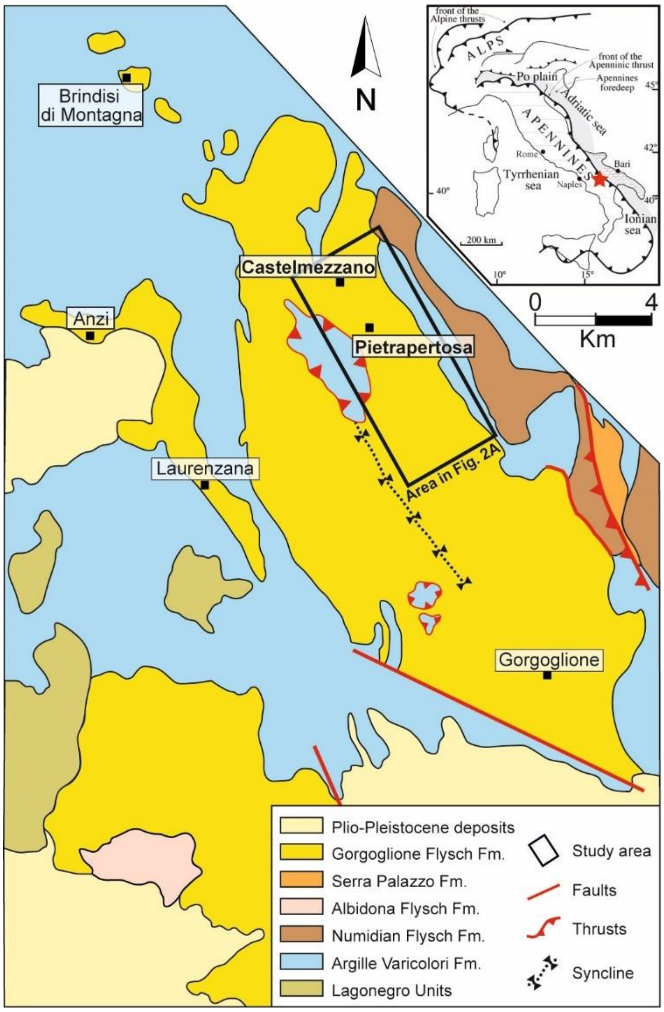

Figure 1

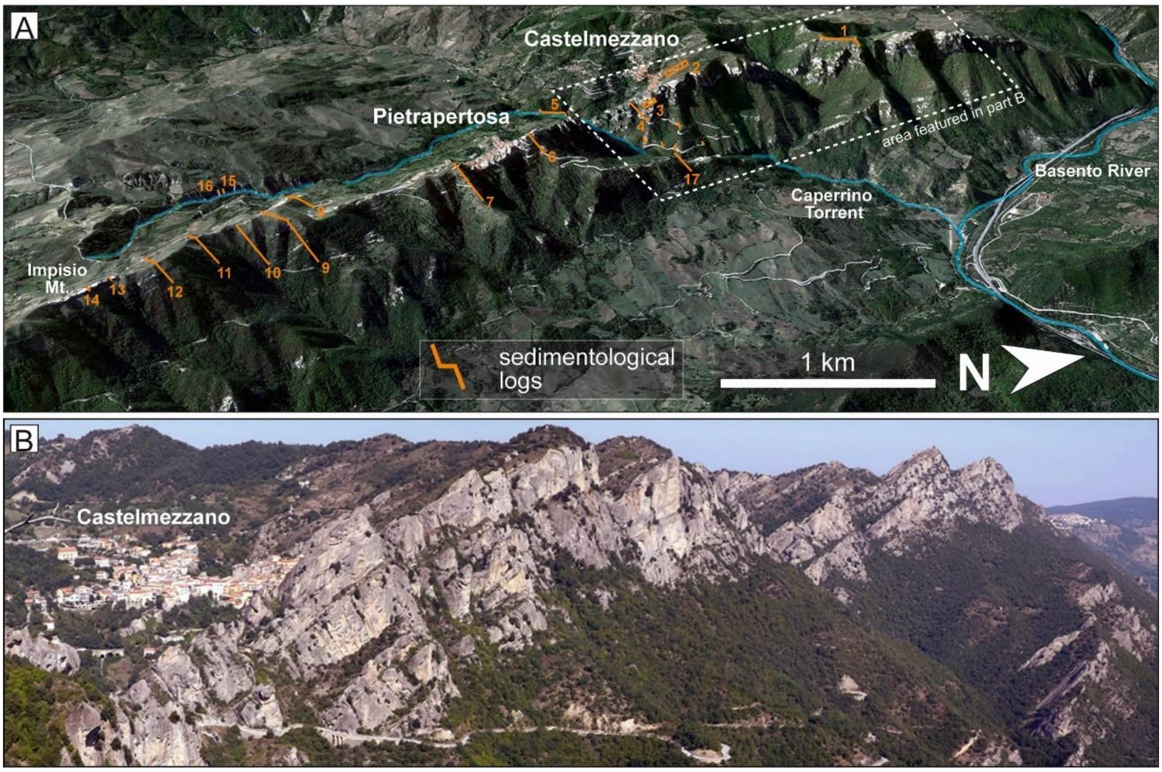
A
Castelmezzano
Pietrapertosa
area featured in part B
Basento River
Caperrino Torrent
Impisio Mt.
1
2
3
4
5
6
7
8
9
10
11
12
13
14
15
16
17
sedimentological logs
1 km
N
B
Castelmezzano

Figure 2

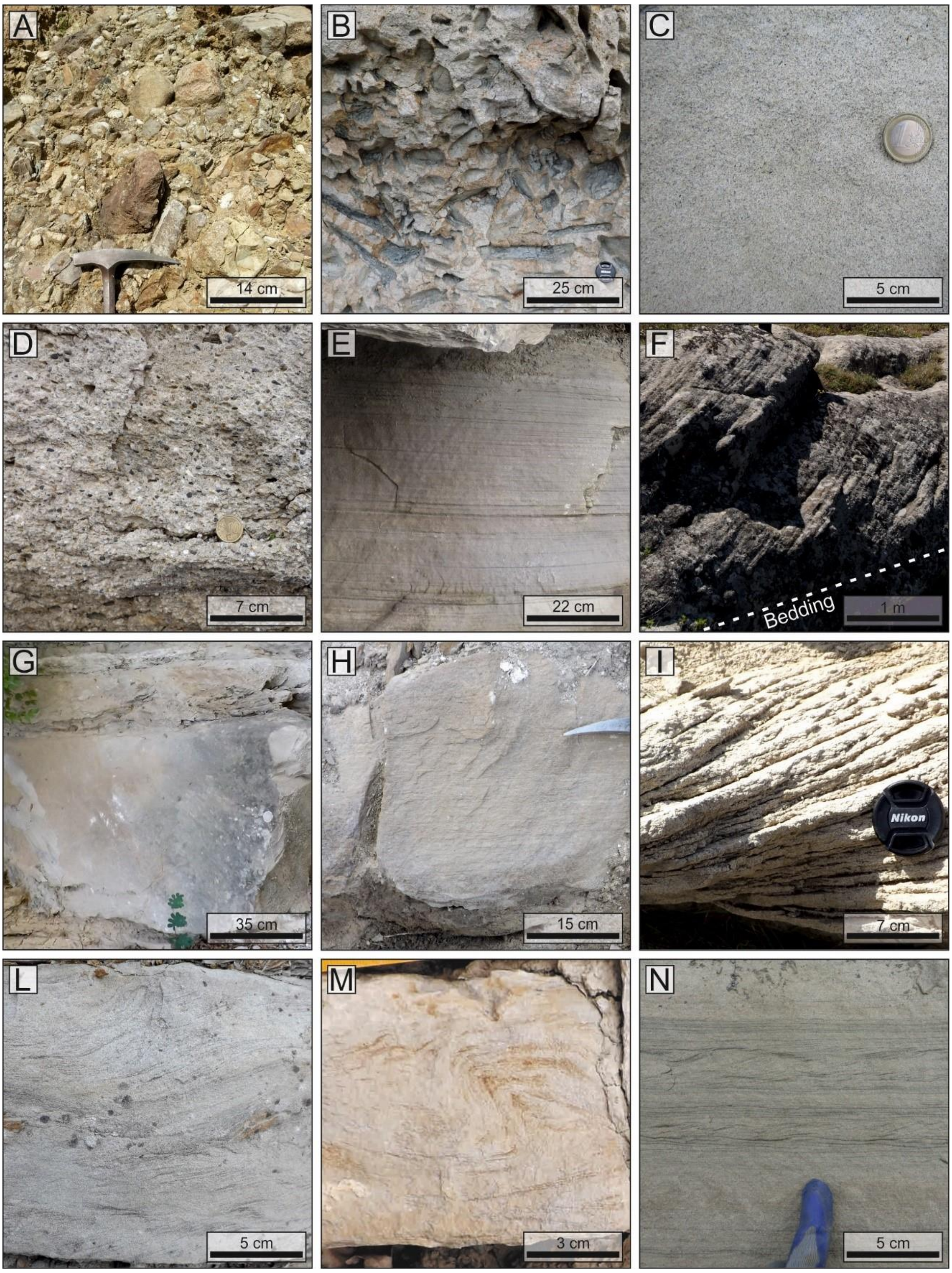
A
14 cm
B
25 cm
C
5 cm
D
7 cm
E
22 cm
F
Bedding
1 m
G
35 cm
H
15 cm
I
Nikon
7 cm
L
5 cm
M
3 cm
N
5 cm

Figure 3

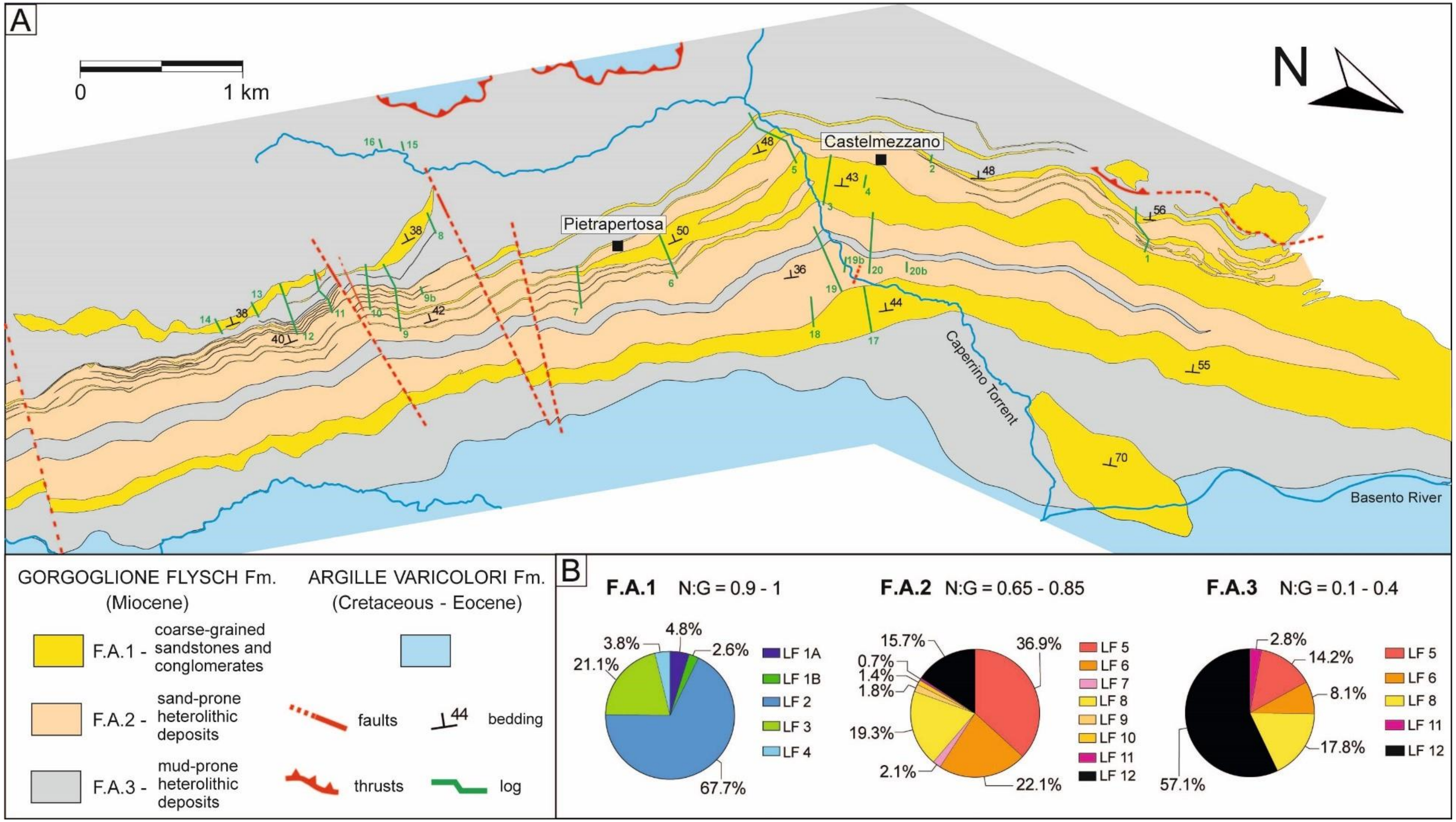
A
0
1 km
N
Castelmezzano
Pietrapertosa
Caperrino Torrent
Basento River
GORGOGLIONE FLYSCH Fm.
(Miocene)
ARGILLE VARICOLORI Fm.
(Cretaceous - Eocene)
F.A.1 - coarse-grained sandstones and conglomerates
F.A.2 - sand-prone heterolithic deposits
F.A.3 - mud-prone heterolithic deposits
faults
thrusts
bedding
log
B
F.A.1 N:G = 0.9 - 1
F.A.2 N:G = 0.65 - 0.85
F.A.3 N:G = 0.1 - 0.4
LF 1A
LF 1B
LF 2
LF 3
LF 4
LF 5
LF 6
LF 7
LF 8
LF 9
LF 10
LF 11
LF 12
4.8%
3.8%
2.6%
21.1%
67.7%
15.7%
36.9%
0.7%
1.4%
1.8%
19.3%
2.1%
22.1%
2.8%
14.2%
8.1%
17.8%
57.1%

Figure 4

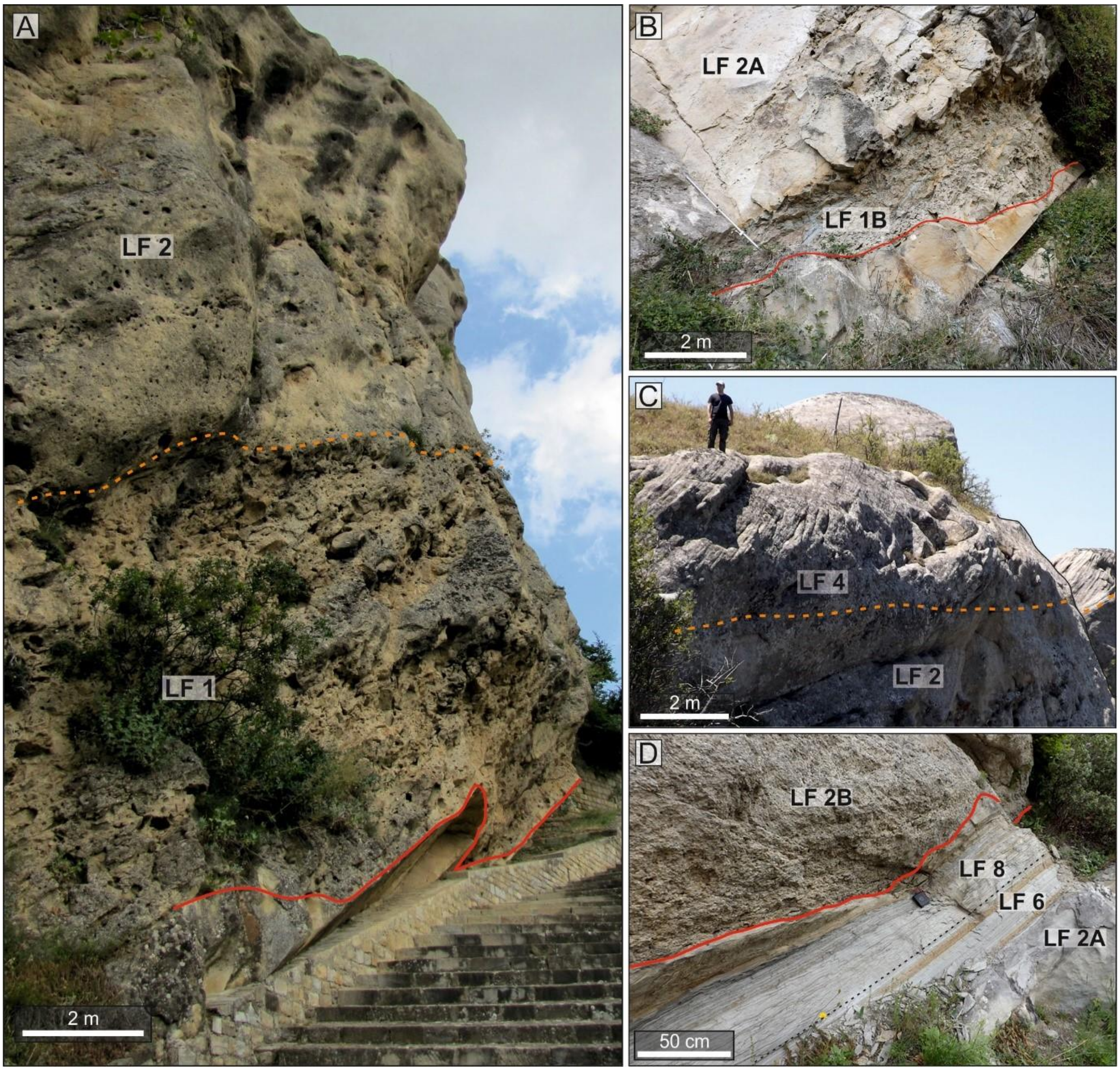

Figure 5

1136 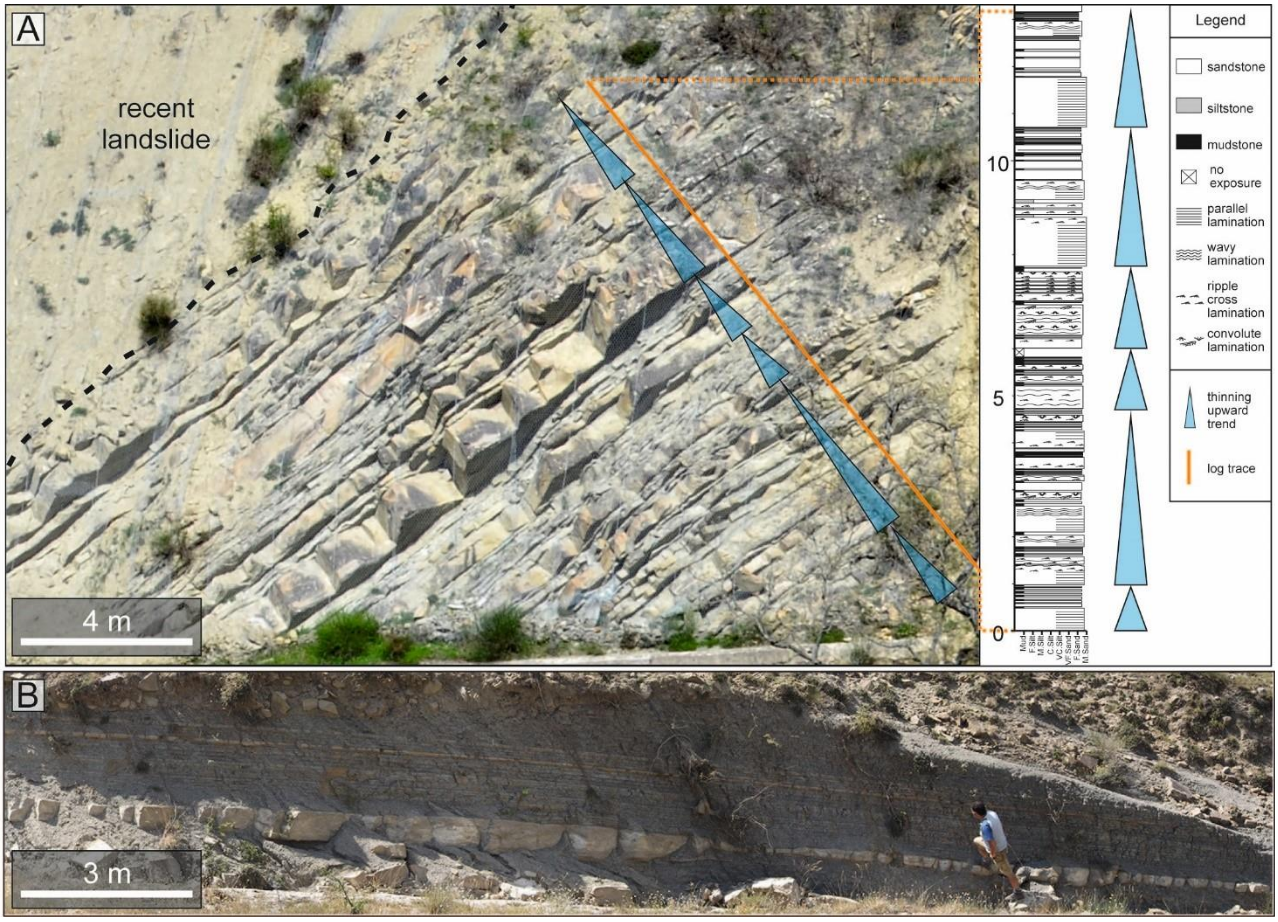

1137 *Figure 6*

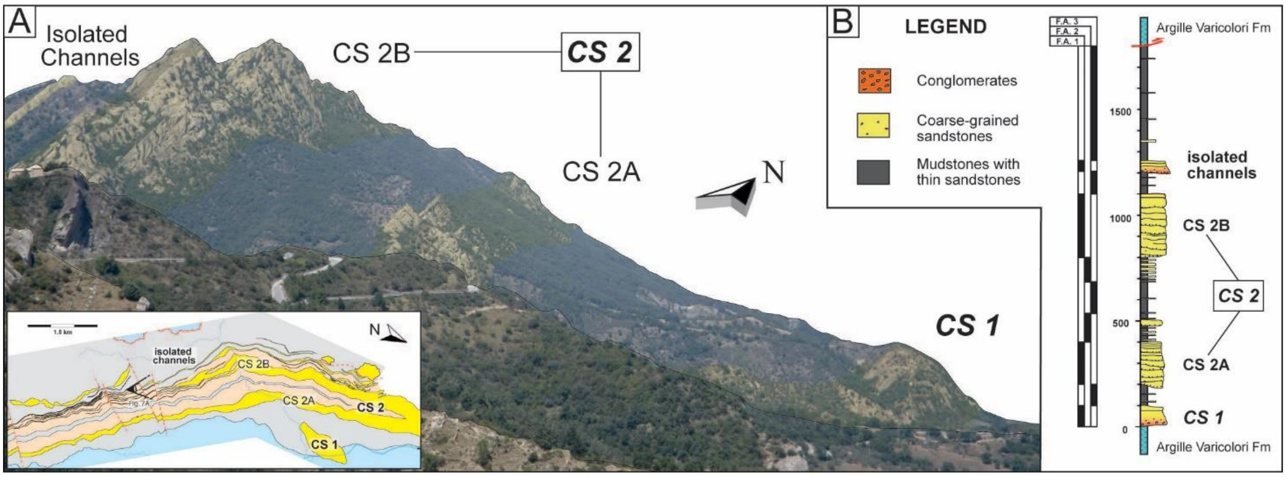
A
Isolated Channels
CS 2B
CS 2
CS 2A
N
CS 1
isolated channels
CS 2B
CS 2A
CS 2
CS 1
B
LEGEND
Conglomerates
Coarse-grained sandstones
Mudstones with thin sandstones
F.A. 3
F.A. 2
F.A. 1
Argille Varicolori Fm
1500
1000
500
0
isolated channels
CS 2B
CS 2
CS 2A
CS 1
Argille Varicolori Fm

Figure 7

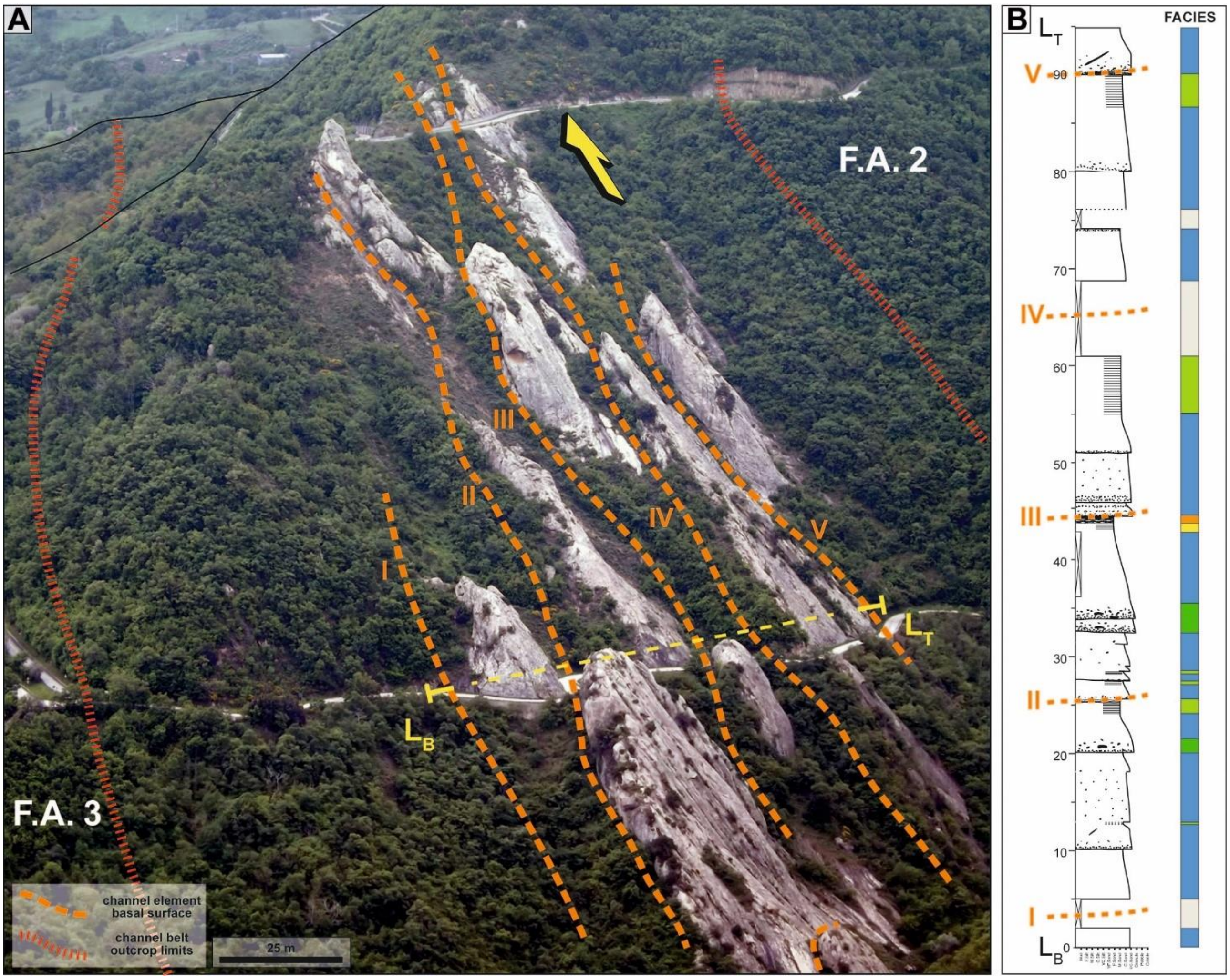
A
F.A. 2
F.A. 3
I
II
III
IV
V
LB
LT
channel element basal surface
channel belt outcrop limits
25 m
B
FACIES
0
10
20
30
40
50
60
70
80
90

Figure 8

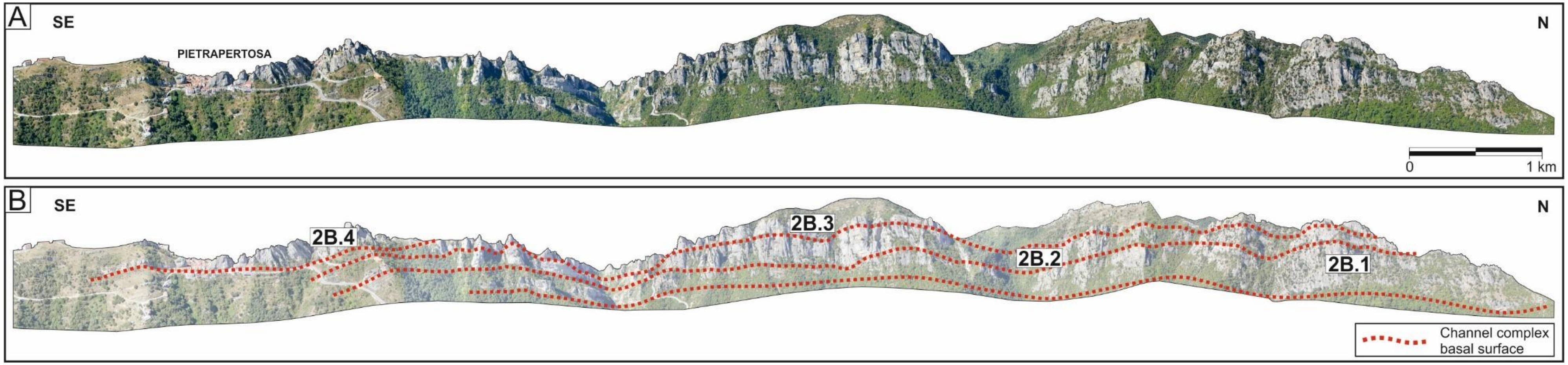
A
SE
N
PIETRAPERTOSA
0
1 km
B
SE
N
2B.4
2B.3
2B.2
2B.1
Channel complex basal surface

Figure 9

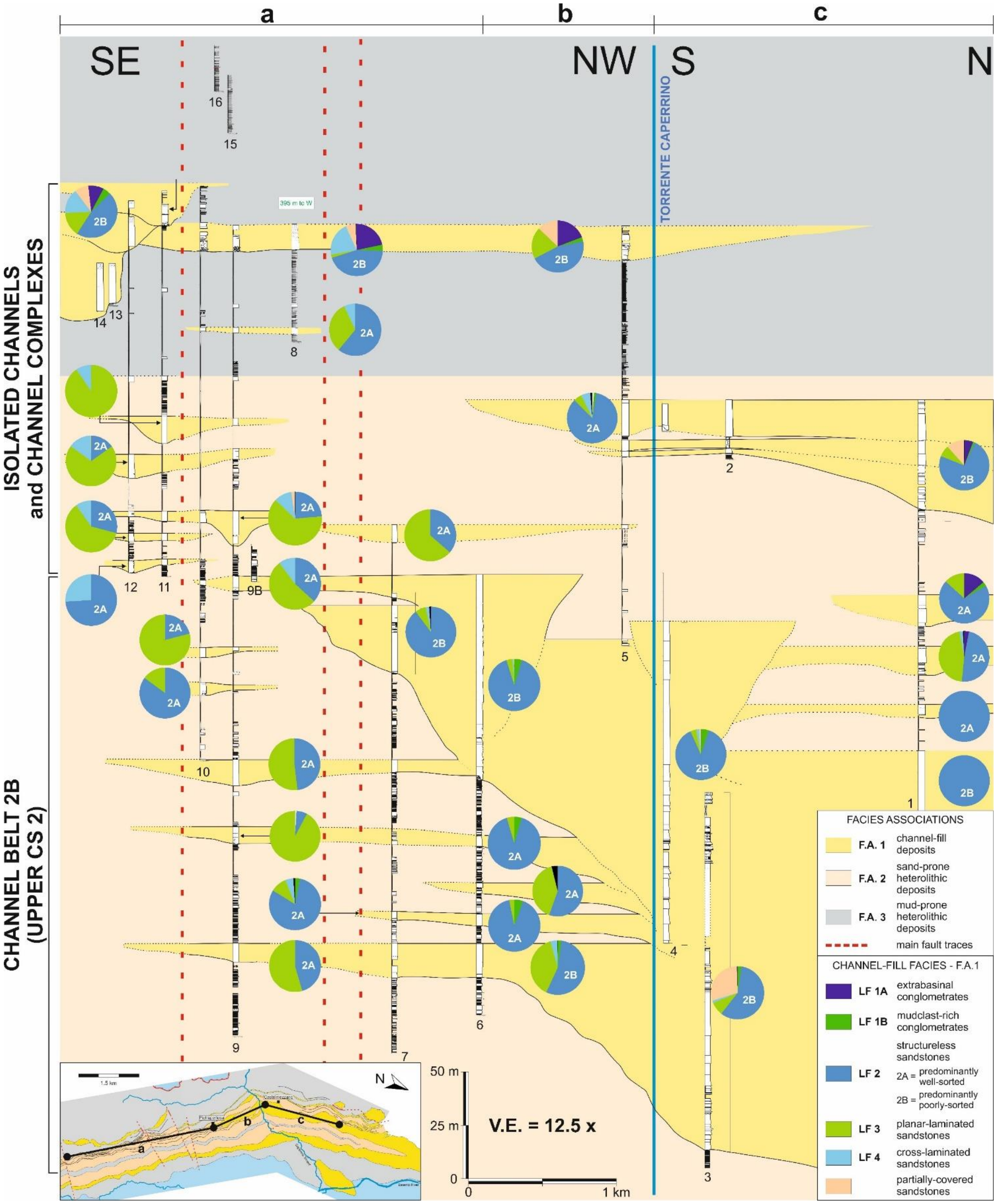
a
b
c
SE
NW
S
N
TORRENTE CAPERRINO
ISOLATED CHANNELS and CHANNEL COMPLEXES
CHANNEL BELT 2B (UPPER CS 2)
395 m to W
50 m
25 m
0
0
1 km
V.E. = 12.5 x
FACIES ASSOCIATIONS
F.A. 1 channel-fill deposits
F.A. 2 sand-prone heterolithic deposits
F.A. 3 mud-prone heterolithic deposits
main fault traces
CHANNEL-FILL FACIES - F.A.1
LF 1A extrabasinal conglometrates
LF 1B mudclast-rich conglometrates
LF 2 structureless sandstones
2A = predominantly well-sorted
2B = predominantly poorly-sorted
LF 3 planar-laminated sandstones
LF 4 cross-laminated sandstones
partially-covered sandstones

Figure 10

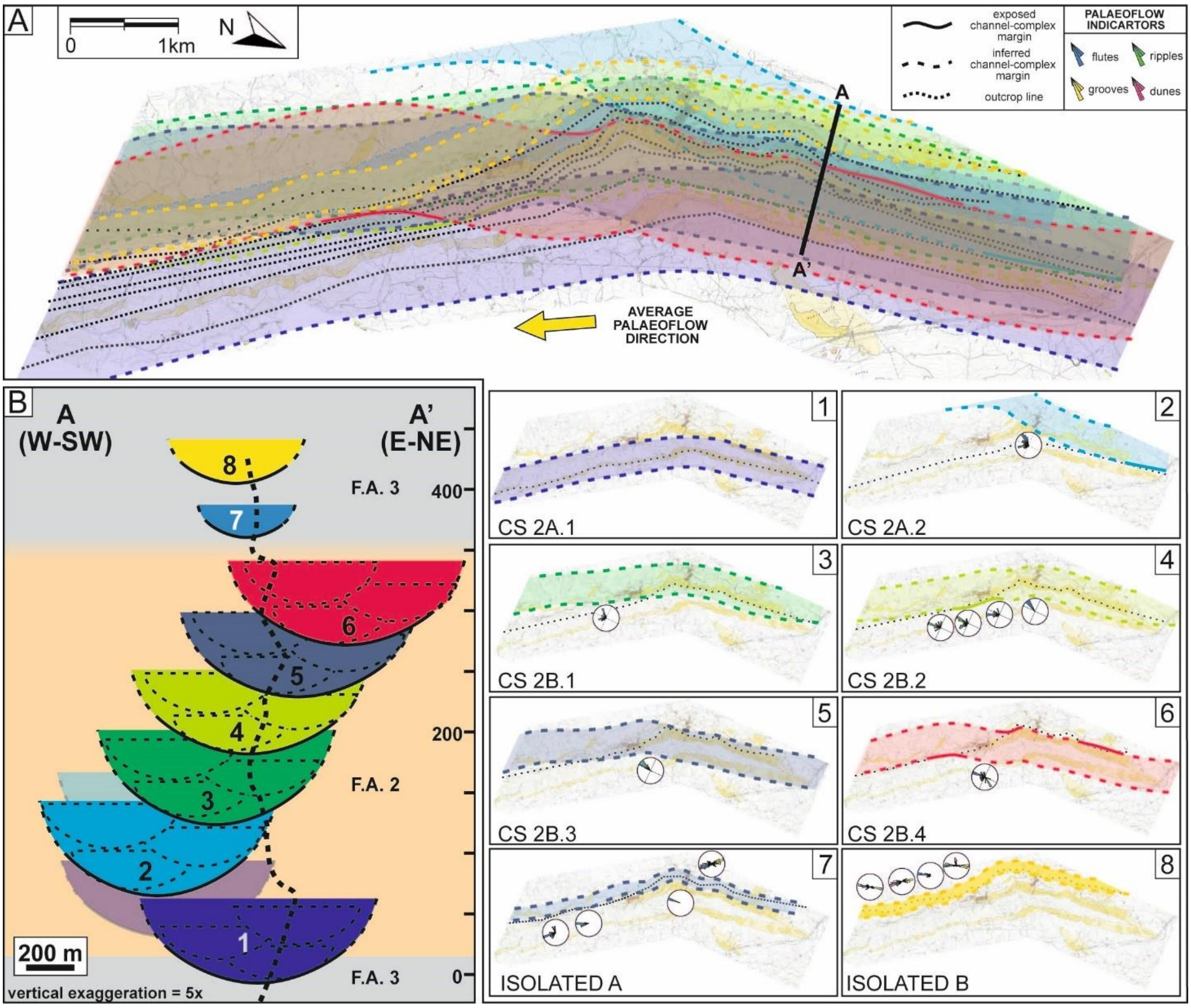
A
0
1km
N
exposed channel-complex margin
inferred channel-complex margin
outcrop line
PALAEOFLOW INDICARTORS
flutes
ripples
grooves
dunes
A
A'
AVERAGE PALAEOFLOW DIRECTION
B
A (W-SW)
A' (E-NE)
F.A. 3
400
F.A. 2
200
F.A. 3
0
200 m
vertical exaggeration = 5x
8
7
6
5
4
3
2
1
CS 2A.1
CS 2A.2
CS 2B.1
CS 2B.2
CS 2B.3
CS 2B.4
ISOLATED A
ISOLATED B

Figure 11

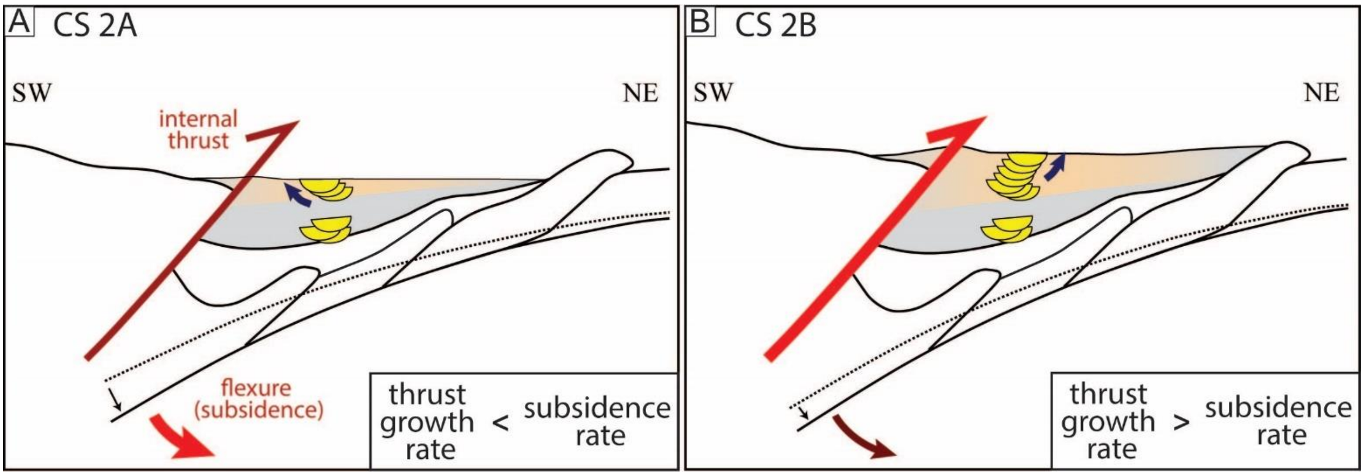
A
CS 2A
SW
NE
internal
thrust
flexure
(subsidence)
thrust
growth
rate
<
subsidence
rate
B
CS 2B
SW
NE
thrust
growth
rate
>
subsidence
rate

Figure 12

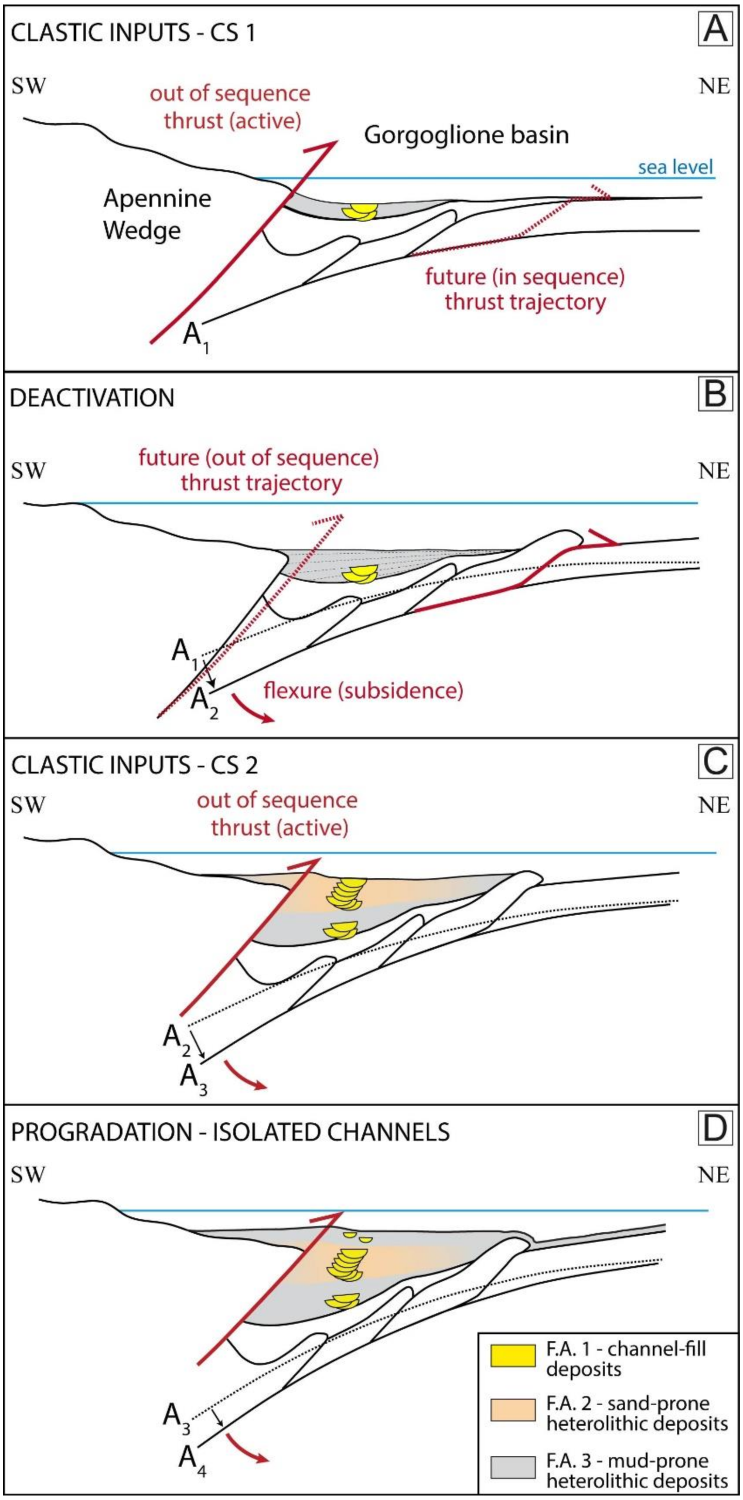
CLASTIC INPUTS - CS 1
A
SW
NE
out of sequence
thrust (active)
Gorgoglione basin
sea level
Apennine
Wedge
future (in sequence)
thrust trajectory
A_1
DEACTIVATION
B
SW
NE
future (out of sequence)
thrust trajectory
A_1
A_2
flexure (subsidence)
CLASTIC INPUTS - CS 2
C
SW
NE
out of sequence
thrust (active)
A_2
A_3
PROGRADATION - ISOLATED CHANNELS
D
SW
NE
A_3
A_4
F.A. 1 - channel-fill deposits
F.A. 2 - sand-prone heterolithic deposits
F.A. 3 - mud-prone heterolithic deposits

Figure 13

CAPTIONS

Table 1 – Operative lithofacies recognized in the Gorgoglione Flysch Formation. Turbidite divisions are from Bouma (1962), Lowe (1982) and Mutti (1992).

Figure 1 - Schematic geological map of the main outcrops of the GF Formation (from Critelli and Loiacono 1988, modified). Proximal facies are recognized in the western outcrops, at Brindisi di Montagna, Anzi and Laurenzana, where the GF is characterized by very coarse-grained sandstones and conglomerates derived from internal paleogeographic domains. The main depocentral area is located to the east, between the towns of Castelmezzano and Gorgoglione, where the GF succession reaches a thickness of nearly 2000 m.

Figure 2 – A) Overview of the study area (see Fig. 1 for location), extending for about 15 km between the Basento River to the north and the Impisio Mountain to the south. Multiple stratigraphic sections have been measured across the outcrop belt, in order to characterize spatial changes in architectural and sedimentological features. B) The monoclinal configuration of the GF formation, dipping towards SW of nearly 40°, which defines the spectacular cliffs that inspired the local name of "Lucanian Dolomites" (location in A).

Figure 3 – Lithofacies of the GF formation. (A) LF 1A, matrix-supported extrabasinal conglomerates. (B) LF 1B, mudclasts conglomerate. (C) LF 2A, clean, poorly-sorted coarse-grained sandstones. (D) LF 2B, very coarse-grained sandstones with dispersed granule- to pebble-sized clasts. (E) LF 3, planar-laminated sandstones. (F) LF 4, coarse-grained sandstones with large-scale cross-stratification. (G) LF 5, massive, medium-grained sandstones (Bouma Ta). (H) LF6, planar-laminated, medium-bedded sandstones (Bouma Tb). (I) LF 7, cross-stratified, medium bedded sandstones. (L) LF 8, ripple cross-laminated, thin-bedded sandstones (Bouma Tc). (M) LF 9, convoluted, fine-grained sandstones. (N) LF 10, alternating planar-laminated (Tb) and ripple cross-laminated (Tc) fine-grained sandstones.

Figure 4 – A) Geological map of the study area (see Fig. 1 for location), showing the distribution of the three main facies associations. The turbidite succession is affected by post-depositional deformation characterized by large-scale tilting and by smaller structures of various ages (e.g., normal faults in the southern portion of the study area). The GF formation is bounded unconformably at the base and tectonically at the top by the Argille Varicolori Formation (Cretaceous-Eocene). B) Pie charts of the relative proportions of sedimentary facies (codes as in Table 1) across the study area, calculated as thickness percentages from all the logged sections. Net-to-gross values (N:G) represent the cumulative thickness of sandstones versus the total thickness.

Figure 5 – Channel-fill deposits (F.A.1). (A) Matrix-supported, mixed extrabasinal and intrabasinal conglomerates (LF 1) overlaid by poorly-sorted structureless sandstones (LF 2B), characteristic of channel axis (B) Basal lag conglomerates almost entirely constituted of mudclasts (LF 1B) and overlain by clean massive sandstones (LF 2A), characteristic of channel off-axis. (C; D) Variable character of the top of channel-fill sequences. In (C), thick structureless sandstones (LF 2) are abruptly overlain by large-scale cross-stratified

sandstones (LF 4). Conversely, in (D) amalgamated, fine-grained structured sandstones (LF 6 and LF 8) are truncated by an extensive erosional surface marking the beginning of the subsequent channel-fill sequence.

Figure 6 – Heterolithic, out-of-channel deposits. A) Thinning-upward trends (blue triangles) within the sand-prone heterolithic deposits of F.A.2. The section is partially covered by collapsed material. B) Lenticular bed composed of massive sandstones (LF 5) embedded in mud-prone heterolithic deposits of F.A.3

Figure 7 – A) Panoramic view of the GF succession in the study area, showing the main large-scale architectural units: channel complex-sets and isolated channels (see inset map for location). In this study, channel belts 2A and 2B are considered as parts of the same migrating channel complex-set, referred to as "CS 2". B) Representative log of the GF succession, measured along the Caperrino Torrent, between the towns of Pietrapertosa and Castelmezzano. Black and with bar shows the dominant facies association along the logged section.

Figure 8 – A) Stacked elementary channels of CS 2A, exposed along the valley of the Caperrino Torrent. CS 2A overlies a prominent erosional surface, deeply incisional into mud-prone heterolithic deposits (F.A.3). The regional paleoflow is towards SSE (yellow arrow). B) Sedimentological log L_B - L_T of the CS 2A (see Fig. 6A for the log legend and Fig. 4B for the facies legend). This section exposes the stacked channel axes, which are dominated by pebble-rich structureless sandstones (LF 2B), with subordinate clean massive sandstones (LF 2A) and planar laminated sandstones (LF 3), locally capped by large-scale cross stratified sandstones (LF4).

Figure 9 – Aerial photopanel (A) and interpretation (B) of the northern sector of the CS 2B. Four amalgamated channel complex, 60 to 85 m thick, have been recognized, separated by major erosional surfaces laterally traceable for about 4 km across the study area. Channel complexes show an abrupt lateral thinning toward S-SE. The apparent elongated shape of the channel belt is due to the highly oblique orientation of the outcrops, which is nearly parallel to the regional palaeoflow direction (toward SSE).

Figure 10 – Correlation panel of the upper portion of the GF succession exposed in the study area, showing the spatial distribution of the four channel-fill facies (F.A.1). Location in the inset geological map; offset of post-depositional faults (dashed red lines) has been removed. The panel includes the CS 2B and the upper isolated channels and channel complexes. CS 2B is comprised of amalgamated, laterally-offset stacked channel complexes, resulting in a composite architecture at the large scale. Channel-fill deposits in the northern sector are dominated by poorly-sorted structureless sandstones (LF 2B) and exhibit a lateral transition towards SE into less-amalgamated and laterally-persistent sandbodies with abundant well-sorted massive and planar-laminated sandstones (LF 2A and LF 3, respectively). This lateral trend has been interpreted to reflect a progressive transition from channel axis to channel margin facies. The correlation panel highlights the upward change in the character of the heterolithic deposits, which passes from sand-prone (F.A.2) to mud-prone (F.A.3). Vertical exaggeration 12.5 times.

Figure 11 – A) Reconstruction of the planform geometry of the channel complexes comprising the CS 2 and of two isolated channel elements in the upper part of the GF succession. The topographic map in the background represents the distribution of the channel-fill deposits in the study area. Due to the lack of exposure of both of the CS 2 channel complex-set margins, the real width of its component channel complexes cannot be measured directly. Accordingly, for their representation, an average width of 1 km has been considered from literature (Sprague et al., 2005; Stright et al., 2014). The regional paleoflow was roughly SE-ward. CS 1 is not represented due to the lack of paleoflow measurements and discontinuous exposures of channel fill deposits. B) Cross section orthogonal to regional paleoflow direction (location in A), showing the stacking pattern of the different units. The dotted black line shows the outcrop profile in the transect line. The CS 2 is dominated by vertical aggradation, with a characteristic "zig-zag" stacking pattern of the component units.

Figure 12 - Schematic representation of the progressive lateral migration of the CS 2 depocenter in GF basin, resulting in the "zig-zag" stacking pattern. This characteristic migration pattern might be interpreted as the net result of the competition between the growth of the internal thrust and the regional subsidence, which created accommodation space at a constant rate and promoted aggradation. A) When the growth rate of the trust was lower than the subsidence rate, the fast eastward roll-back at the hinge of the subduction zone favored the migration of the channel system depocentre towards SW; B) Conversely, when the thrust growth rate became higher than the subsidence rate, the push of this regional tectonic structure forced the CS 2 to shift towards NE.

Figure 13 – Main stages of the GF turbidite system evolution, developed during the Late Miocene in a thrust-bounded piggy-back basin of the Southern Apennines. Significant accommodation space was formed as a consequence of the increasing subsidence of the basin, associated to ongoing subduction. A) The early activity of the internal thrusts determined increasing gradients in the orogenic hinterland, promoting the establishment of a slope environment. High slope gradients facilitated the initiation and development of the incisional gravity flows that built up the CS 1. B) The subsequent activation of the outer thrusts progressively configured a narrow basin, marking the end of CS 1 sedimentation and promoting the deposition of a thick package of F.A.3 deposits. Decreasing slope gradients in the orogenic hinterland led to a gradual restoration of a base-of-slope environment. C) The re-activation of the internal thrusts restored the coarse clastic inputs in the basin and fostered the development of the CS 2. D) Ongoing coarse-grained inputs, combined with a gradual increase of the basinal slope gradient, promoted the formation of progressively more incisional turbidity currents. Accordingly, the amalgamated, weakly confined channels of the CS 2 gradually evolved into isolated, strongly-confined channels. This upward change in channel architectural style is interpreted to represent the progradation of a slope channel system over a weakly-confined, sand-prone channel system on the near base-of-slope.

FACIES	LITHOLOGY	GRADING	THICKNESS	PHYSICAL STRUCTURES	LITHOLOGICAL ACCESSORIES	BASAL SURFACE PROPERTIES	TURBIDITE DIVISION	PROCESS INTERPRETATION
LF 1 Matrix-sup-ported con-glomerates	LF 1A: pebble to boulder extrabasinal conglomerate with coarse to very coarse sandstone matrix LF 1B: pebble to cobble mudclast conglomerate with very coarse sandstone matrix	Typically ungraded and disorganized. Local weak normal grading	LF 1A usually 2.1 - 2.9 m range 0.4 - 5.2 m LF 1B usually 0.5 - 2.3 m range 0.2 - 3.4 m	Chaotic internal organisation. Sole structures (flute and groove casts)	LF 1A: sub-rounded to sub-angular extraformational clasts, 6 - 80 cm in diameter (average 20 cm). LF 1B: angular to sub-rounded (mainly disk-shaped) mudclasts, 1 - 30 cm in diameter. Local substrate blocks up to 1.5 m	Sharp and irregularly-shaped, often concave upward, erosional	-	Lag deposits from bypassing high-density turbidity currents. Bed-load transport from highly-incisional flows. LF 1B mudclasts incorporated into the bypassing flow after turbulent scouring of cohesive mud substrate
LF 2 Structureless, thick bedded sandstones	LF 2A: medium to very coarse, well-sorted sandstone LF 2B: medium to very coarse, poorly-sorted sandstone	Ungraded to crudely normally graded	usually 0.9 - 2 m range 0.6 - 5.5 m Amalgamated beds locally form units up to 53 m thick	Structureless, with local dewatering features	LF 2A: disk-shaped mudclasts, 1 to 6 cm in diameter LF 2B: extrabasinal clasts, up to 5 cm in diameter, locally in lags	Sharp to undulating. Commonly amalgamated, marked by aligned mudclasts. Locally gradational with	S3 ; F5	Rapid deposition of suspended sediment from collapsing, high-density currents with high se- diment fallout rates, suppressing bed-load traction

						underlying facies		
LF 3 Planar-laminated, thick bedded sandstones	Medium to coarse, clean sandstone	Ungraded to normally-graded	usually 0.6 - 1.7 m range 0.4 - 3.25 m Amalgamated beds locally form units up to 11.2 m thick	Closely- spaced planar laminations	Aligned mudclasts, up to 5 cm in diameter	Planar. Commonly gradational with underlying facies. Locally amalgamated, marked by aligned mudclasts	T_t ; F7	Deposition from high-concentration near-bed layers (traction carpets) generated by rapid sediment-fallout and progressive traction beneath high-density flows
LF 4 Large-scale, cross-stratified sandstones	Medium to coarse, clean sandstone	Normally graded	usually 0.6 - 1.4 m range 0.3 - 6.4 m	Multiple sets of large-scale 3D cross stratifications	Local seams of broadly aligned cm-sized rip-up mudstone clasts separating different bedsets	Commonly sharp, locally gradational	F6	Gradual decrease of confinement of sandy dense flows, leading to fast and lower-concentration, fully turbulent tractive flow
LF 5 Massive, thin-bedded sandstones	Fine to medium sandstone	Typically ungraded or slightly normally graded	1 - 45 cm (occasionally up to 1.3 m)	Structureless, with occasional planar laminations or ripples at the top	Occasional cm-sized aligned mudclasts. Rare extrabasinal clasts up to 1 cm	Typically planar; sporadically weakly erosional, ornamented by small flutes	T_a, with local T_{ab}, T_{abc}	Rapid deposition from high density turbidity currents with very high sediment-fallout rates, preventing the formation of tractive features

LF 6 Planar laminated, thin-bedded sandstones	Fine to medium, clean sandstone	Ungraded to normally graded	6 - 75 cm (occasionally up to 90 cm)	Closely- spaced planar laminations, with local ripples or wavy laminations at the top	None	Planar	T_b, with local T_{bc}	a) deposition from low amplitude bed waves in waning and dilute, low-density flows, under low suspension fallout rates; b) deposition from traction carpets beneath high-density flows
LF 7 Cross laminated, thin-bedded sandstones	Fine to medium, clean sandstone	Ungraded to normally graded	12 - 64 cm (occasionally up to 87cm)	Small- to medium-scale, low-angle cross stratification, with stratasets ranging from 22 to 60 cm thick	None	Planar, with undulated tops	-	Deposition from dilute flows, with very low sediment fallout rates
LF 8 Ripple cross laminated, thin-bedded sandstones	Predominantly fine, clean sandstone, sometimes up to medium sandstone	Normally graded from fine sandstone at the base to siltstone	1 - 45 cm (occasionally up to 80 cm)	Ripples or wavy laminations	None	Planar, with undulated tops	T_c, with local T_{cd}	Deposition from waning, relatively diluted and fully turbulent suspensions, with low rates of sediment fallout
LF 9 Convoluted,	Predominantly fine, clean sandstone, sometimes up	Normally graded from fine sandstone at the	3 - 17 cm (occasionally up to 60 cm)	Convolute laminations	None	Planar, with undulated tops	T_c	Very rapid deposition of fine-grained sediment, triggering syn- and

thin-bedded sandstones	to medium sandstone	base to siltstone						port-depositional upward dewatering
LF 10 Vacillatory turbidites	Fine to medium, clean sandstone	Ungraded	9 - 48 cm (occasionally up to 83 cm). Rare amalgamation to form units up to 2.3 m thick	Alternating planar laminations and ripples or wavy laminations	None	Planar, with undulated tops	T_{bcbc}	Flow regime fluctuations of a tractive, low-density turbidity current
LF 11 Deformed deposits	Fine- to medium sandstone blocks or beds in a mud-stone or sandstone matrix	Ungraded	32 - 250 cm	Folded and con-torted beds with minor thrusts and dewatering	Locally mudclasts up to 20 cm in diameter	Sharp	-	Slumping of heterolithic packages
LF 12 Mudstone	Mudstone or very fine silt-stone	Ungraded or slightly graded	1 - 16 cm (locally up to 30 cm)	Massive, occasionally finely laminated	None	Sharp or gradational with under-lying strata	T_d, T_e	Deposition en masse or incrementally, by floc segregation settling and fallout from dilute low-density turbidity currents